Title

Menthol in electronic cigarettes: A contributor to respiratory disease?

Authors

Nair, Vijayalekshmi
Tran, Malcolm
Behar, Rachel Z
et al.

Publication Date

2020-11-01

DOI

10.1016/j.taap.2020.115238

Peer reviewed

Menthol in Electronic Cigarettes: A Contributor to Respiratory Disease?

Vijayalekshmi Nair[1], Malcolm Tran[1], Rachel Z. Behar[1], Song Zhai[2], Xinping Cui[2], Rattapol Phandthong[1], Yuhuan Wang[1], Songqin Pan[3], Wentai Luo[4], James F. Pankow[4], David C. Volz[5,] and Prue Talbot[1]*

[1]Department of Molecular, Cell and Systems Biology, University of California, Riverside, CA *92521,* USA

[2]Department of Statistics, University of California, Riverside, CA *92521,* USA

[3]Proteomics Facility IIGB, University of California, Riverside, CA *92521,* USA

[4]Department of Civil and Environmental Engineering, Portland State University, Portland, Oregon

[5]Department of Environmental Sciences, University of California, Riverside, CA *92521,* USA

The first two authors contributed equally to this work

* Corresponding Author:

Prue Talbot

Telephone: 951-850-7783

talbot@ucr.edu

ABSTRACT

Menthol is widely used in tobacco products. This study compared the effects of menthol on human bronchial epithelium using submerged cultures, a VITROCELL® cloud chamber that

provides air liquid interface (ALI) exposure without solvents or heating, and a Cultex ALI system that delivers aerosol equivalent to that inhaled during vaping. In submerged culture, menthol significantly increased calcium influx and mitochondrial reactive oxygen species (ROS) via the TRPM8 receptor, responses that were inhibited by a TRPM8 antagonist. VITROCELL® cloud chamber exposure of BEAS-2B monolayers increased mitochondrial protein oxidation, expression of the antioxidant enzyme SOD2, activation of NF-κB, and secretion of inflammatory cytokines (IL-6 and IL-8). Proteomics data collected following ALI exposure of 3D EpiAirway tissue in the Cultex showed upregulation of NRF-2-mediated oxidative stress, oxidative phosphorylation, and IL-8 signaling. Across the three platforms, menthol adversely effected human bronchial epithelium in a manner that could lead to respiratory disease.

Keywords: Menthol, air-liquid interface exposure, reactive oxygen species, inflammation, TRPM8, respiratory cells, electronic cigarettes

INTRODUCTION

Flavor chemicals are widely used in tobacco products, including electronic cigarettes (ECs) (Behar et al., 2018; Hua et al., 2019; Lisko et al., 2014; Tierney et al., 2016), and numerous attractive flavors have contributed to the rapid rise in the popularity of ECs in the US (U.S. Department of Health and Human Services, 2016; Miech et al., 2019; U.S. Department of Health and Human Services, 2016). While most flavor chemicals in consumer products are "generally regarded as safe" (GRAS), the Flavor and Extracts Manufacturers Association's (FEMA) GRAS designation pertains only to ingestion, not inhalation (Hallagan, 2014). Because the data on flavor chemical ingestion cannot be directly translated to inhalation, the health consequences of short-and long-term inhalation of flavor chemicals in ECs remain largely uncharacterized. This problem is compounded by the lack of validated methods for determining the effects of EC flavor chemicals and their reaction products on the respiratory system.

Menthol is often used in ECs (Behar et al., 2018; Hua et al., 2019) and is the only flavor chemical permitted in tobacco cigarettes under the Family Smoking Prevention and Tobacco Control Act (2009). EC refill fluids and conventional cigarettes sometimes contain menthol, even when they are sold as non-mentholated (Behar et al., 2018; Henderson, 2019; Omaiye et al., 2018). Menthol produces a cooling effect upon binding to the TRPM8 receptor (Transient Receptor Potential Melastatin 8), a cation channel with selectivity for calcium (Peier et al., 2002). Menthol is used in tobacco products to impart flavor and to reduce the harshness of tobacco smoke, making inhalation easier for novices (DeVito et al., 2019; Willis et al., 2011). Mentholated ECs may facilitate the initiation of smoking, increase nicotine dependence, and increase progression to conventional cigarette smoking (Food and Drug Administration, 2011; Nonnemaker et al., 2013; Villanti et al., 2017). Mentholated tobacco cigarettes also reduce cessation rates when compared to non-mentholated tobacco cigarettes (Delnevo et al., 2011). Mentholated tobacco cigarettes are widely distributed among African American and adolescent smokers, and are used more often by women than men (Food and Drug Administration, 2011).

In a weight of evidence analysis on conventional cigarettes, it was concluded that menthol is not associated with a disease risk to the user (Food and Drug Administration, 2011). However, this conclusion was based on comparisons of mentholated and non-mentholated conventional cigarettes, and it may not pertain to ECs, which often have much higher concentrations of menthol than those in food and other consumer products, including tobacco cigarettes (Hua et al., 2019; Tierney et al., 2016). As examples, in mentholated tobacco cigarettes the concentration of menthol ranges between 0.52- 4.19 mg/cigarette (Ai et al., 2016) and averages 4.75 mg/cigarette (Paschke et al., 2017). In contrast, menthol concentration in one EC refill fluid was 85 mg/mL (Behar et al., 2017) and 15 mg/mL in mint flavored JUUL pods (Omaiye et al., 2018), a brand popular with adolescents (Barrington-Trimis and Leventhal, 2018).

Existing studies indicate a need for further work on the potential for high menthol concentrations in ECs to be associated with disease. For example, in submerged 2-dimensional (2D) cell cultures, EC refill fluids and aerosols had cytotoxic effects on adult and embryonic cells, and these were often associated with flavor chemical concentrations (Bahl et al., 2012; Behar et al., 2017; Hua et al., 2019). Pure menthol was cytotoxic to bronchial epithelium at the concentrations found in EC products when tested *in vitro* with the MTT assay using 2D submerged cell cultures (Behar et al., 2017; Hua et al., 2019). Lin et al., (2018) showed that subchronic exposure of mice to mentholated cigarette smoke induced more inflammation in lungs than smoke from non-mentholated cigarettes. Recently, serious respiratory illness and death have been attributed to EC use, and patients requiring hospitalization have been reported to have “e-cigarette or vaping product use-associated lung injury” (EVALI) (Centers for Disease Control and Prevention, 2019). The etiology of EVALI is not understood, but EC products with high concentrations of flavor chemicals should be investigated as possible causative agents.

The purpose of this study was to determine how menthol affects human bronchial epithelium and to compare responses to menthol across three *in vitro* platforms. In all protocols, the concentrations tested produced no effect in the MTT assay (referred to as the MTT NOAEL – no

observed adverse effect level). In the first protocol, human bronchial epithelium cells (BEAS-2B) were exposed to pure menthol using submerged 2D cultures and oxidative stress and cell proliferation were examined. This protocol also defined the MTT NOEAL and was valuable as an initial screen. In the second approach, BEAS-2B cells were exposed at the air liquid interface (ALI) to pure menthol aerosols produced in a cloud chamber without heat-generated reaction products or the use of solvents (propylene glycol or PG). Endpoints related to oxidative stress and cytokine signaling were examined. In the third protocol, 3D human respiratory epithelium (EpiAirway tissues) was exposed at the ALI to aerosol created by heating e-fluid in an EC, and tissue responses were analyzed using proteomics. This aerosol contained menthol, PG, and reaction products formed during heating and would be equivalent to aerosol inhaled by an EC user. Data were compared across the three platforms and evaluated for their potential to contribute to respiratory diseases. To give relevance to our data in the context of ECs, all tested menthol concentrations were within the range found in EC products (Behar et al., 2017; Hua et al., 2019).

MATERIALS and METHODS

Chemicals

Menthol (catalogue number 63660-1G; Lot: BCBW5590), BCTC (N-(4-tert.-butyl-phenyl)-4-(3-chloropyridin-2-yl) tetrahydropyrazine-1(2H)-carboxamide) and siRNA oligonucleotide against TRPM8 were purchased from Sigma (St. Louis, MO). We performed GC/MS on the menthol, and none of the other 11 known TRPM8 agonists (icilin, linalool, geraniol, hydroxy-citronellal, WS-3, WS-23, Frescolat MGA, Frescolat ML, PMD 38, Coolact P, M8-Ag and Cooling Agent 10) were present.. Bronchial epithelial growth medium (BEGM) was purchased from Lonza (Walkersville, MD). TRPM8 antibody was purchased from Abcam (Cambridge, MA) (catalog number ab109308). SOD2 (catalog number - 13141s) and β-actin (catalog number - 8457s) antibody were purchased from Cell Signaling (Danvers, MA). Anti-NF-

kB p65 (phospho S311) antibody was purchased from Abcam (Cambridge, MA) (catalog number ab194926). MitoSOX dye, Nuclear and Cytoplasmic extraction kit (catalog number 78833), and Lipofectamine RNAiMAX Transfection Reagent were purchased from Thermo Fisher Scientific (Waltham, MA). Mitotimer and GCaMP5 plasmids were purchased from Addgene (Cambridge, MA).

Culture of hPF and A549 cells.

The hPF were purchased from ScienCell (Carlsbad, CA) and cultured on poly-L-lysine coated flasks using the supplier's protocol in complete fibroblast medium containing 2% fetal bovine serum, 1% fibroblast growth serum, and 1% penicillin/streptomycin.

The A549 e cells were purchased from American Type Culture Collection (Manassas, VA). Cells were cultured based on ATCC protocol in F-12K medium containing 10% fetal bovine serum in tissue culture flasks.

Culture and exposure of BEAS-2B Cells and EpiAirway Tissues:

Cell viability, proliferation, calcium influx, and immunodetection of the TRPM8 receptor were done using submerged cultures of BEAS-2B cells (American Type Culture Collection, Rockville, MD). Cell viability, inflammatory response, and oxidative stress were done using ALI exposure in either a cloud chamber (BEAS-2B cells) or Cultex system (EpiAirway).

For submerged cultures, BEAS-2B cells were expanded and grown in serum free BEGM supplemented with growth factors. Culture flasks (Corning, Inc, Corning, NY) were pre-coated with BEBM (Bronchial Epithelial Basal Medium) fortified with collagen (30 mg/ml), fibronectin (10 mg/ml), and bovine serum albumin (BSA, 10 mg/ml). Cells were maintained at 37^{o} C, between 30 and 90% confluence, in a humidified incubator with 5% carbon dioxide. For subculturing, cells were trypsin-dissociated and passaged every 2 to 4 days.

For ALI exposure in the VITROCELL® cloud chamber, 12 mm transwell inserts with a pore size of 0.4µm (Corning NY, USA) were pre-coated with BEBM medium. BEAS-2B cells were plated at 60,000 cells/insert in BEGM medium. After 48 h, basal medium was replaced with fresh medium, medium from the apical layer was removed to enable ALI culture, and the apical layer was washed twice with 0.5 mL phosphate-buffered saline (PBS) immediately before exposure to aerosol in the cloud chamber.

ALI experiments in the Cultex exposure system were done using 3D human EpiAirway tissues (Mat-Tek Corp, Ashland, MA). a 3D mucociliary tissue model consisting of normal, human bronchial epithelial cells (hBEC). EpiAirway was prepared using primary hBECs isolated at Mat-Tek Corp from a 23-year-old Caucasian male non-smoker with no history of respiratory disease. EpiAirway inserts in 12-well plates were equilibrated in 700 µL of AIR-100-ASY assay medium/well for at least 24 hours at 37°C with 5% CO_2 before ALI exposures.

Aerosol generation for exposure of submerged cultures

For submerged culture exposures, aerosol fluids were made in BEAS-2B culture medium (Behar et al., 2016, 2014). Menthol aerosols were produced with fresh unused Vea cartomizers at 2.9 V, 2.1 Ω, and 4W. Lab made refill fluid (6 mL) containing 10 mg/mL of menthol was prepared in 80% propylene glycol and 20% distilled water, and 1mL was loaded into each cartomizer as recommended by the vendor. Puff duration was 4.3 s (Behar et al., 2015), and flow rate was adjusted to produce consistent robust clouds of aerosol which were collected in a round-bottom flask submerged in an ice bath containing BEAS-2B culture medium. Aerosol solutions were made at a concentration of six total puff equivalents (TPE), where one TPE = the number of puffs fully dissolved in 1 mL of culture medium. For each batch, 18 puffs were collected in 3 mL of medium placed in a round bottom flask in an ice bath.

Menthol aerosol exposure using the VITROCELL® Cloud chamber

BEAS-2B cells cultured in transwell inserts were placed in a VITROCELL® Cloud system (VitroCell, Waldkirch, Germany) designed for spatially uniform deposition of aerosols. Stock solutions with various amounts of menthol (0.468 g/mL, 0.156 g/mL, and 0.078 g/mL) were made in dimethyl sulfoxide (DMSO). Working solutions of menthol ranging from 0.15 mg/mL to 3 mg/mL were made immediately before use by dissolving the stock solutions in 0.8% NaCl. 200 µL of the working solutions with or without varying concentrations of menthol were added individually to a VITROCELL® nebulizer and uniform aerosol clouds were made according to the manufacturer's instructions at a flow rate of 200 µL/minute. Control cells were exposed to aerosols created using 200 µL of 0.8% NaCl solutions containing 2 µL of 99% DMSO (equivalent to the amount of DMSO in the highest dose), which was prepared immediately prior to nebulization. Cells were exposed for 1.5 minutes to menthol aerosol nebulized in the cloud chamber, returned to the incubator for 4 h, then exposure was repeated a second time, after which they were placed in the incubator for 24 h.

Menthol EC aerosol exposure at the ALI in a Cultex RFS compact exposure module

ALI exposures to EC generated aerosols were done using EpiAirway 3D tissue models. EpiAirway is a 3D mucociliary tissue derived from tracheal/bronchial epithelial cells from a normal human male (non-smoker). EpiAirway contains basal cells, mucous producing goblet cells, and functional ciliated cells united by tight junctions. When used in conjunction with Cultex ALI technology, the 3D tissues are exposed to treatments apically while pulling nutrients through a semi-porous membrane basally, similar to bronchial epithelial cells in vivo. By incorporating multiple cell types and mimicking EC user exposure conditions, this protocol offers a more accurate representation of acute EC exposure than traditionally used submerged cultures.

A Cultex RFS compact exposure module (Cultex Laboratories GmbH, Hannover, Germany) was used to expose EpiAirway tissues to humidified zero air (control) and EC aerosol using a vacuum pump operating at a flow rate of 5 mL/min/insert. Six cell culture inserts were exposed simultaneously in each experimental run. Direct exposure of cells to EC aerosol was

carried out using a custom designed EC smoking robot (RTI International, North Carolina). The Cultex modular system consisted of the aerosol guiding module and the sampling module. The mouthpiece of the EC inserted into a T connector which fits into the aerosol guiding module. For uniform distribution, the EC aerosol was diluted with humidified zero air (1 L/min) before being drawn into the Cultex® RFS compact exposure system. Puff conditions were: 30 puffs with a puff volume of 55 mL, 4 sec puff duration and 60 sec inter-puff intervals. A programmable pump with a flow control application was used for dispensing aerosol. The aerosol guiding module (in the form of a T connector) was fitted tightly to the sampling module (Cultex RFS compact module) before exposure. The sampling module housed six culture inserts, which were separately supplied with medium. Airflows were maintained and controlled by a mass flow controller (Bronkhorst, Bethlehem, PA). Before exposure, the apical surfaces of the EpiAirway tissues were rinsed once with 500 µL PBS and then transferred to the exposure module containing 3 mL of maintenance medium/well. During each exposure, six tissue samples were exposed individually to EC aerosol diluted with humidified zero air or humidified zero air only. Control tissues were subject to the same procedures as test tissues, and a minimum of three tissue samples were included in each experiment. 24 h after exposure, medium was collected and stored to carry out cytotoxicity assays and ELISAs. EpiAirway tissue in the transwell inserts were used for the MTT assay and proteomics analysis.

TRPM8 protein detection by immunohistochemistry

BEAS-2B cells cultured in chamber slides were fixed with 4% paraformaldehyde in tris-buffered saline (TBS) for 10 minutes. Cells were washed 3x with TBS containing 0.1% tween-20 (TBS/T), and non-specific binding was blocked using 10% donkey serum and 5% BSA in TBST. The cells were rinsed 3x with TBS and incubated at 4^0C for 18 h with a rabbit polyclonal IgG antibody (1:500) specific to human TRPM8 (Abcam, Cambridge, MA). Cells were washed and treated for 1 h at room temperature with an Alexa-Fluor 488 conjugated donkey anti-rabbit IgG secondary antibody (Life Technologies, Carlsbad, CA) diluted 1:400 in the blocking solution.

Nuclei were counter-stained with 6-diamidino-2-phenylindole (DAPI) in TBS (1:1000). Negative controls were treated with secondary antibody only. Images were captured at 60X in the green and blue channels with an integrated CMOS camera on a Nikon Ellipse microscope. FITC and DAPI images were merged using ImageJ software.

MTT assay

Cell viability was measured by reduction of tetrazolium salt methyl thiazoyl tetrazolium (MTT) after 24 h of treatment in submerged culture, after EC aerosol exposure in the Cultex system, and 24 h after the second menthol aerosol exposure in the VITROCELL® ALI system. For each platform, three independent experiments were performed. Means and standard errors of the mean (SEM) were used to produce concentration-response curves.

For submerged BEAS-2B cultures, the MTT assay was performed as described previously (Behar et al., 2018). 4,500 cells/well in 96-well plates were treated with menthol solution or aerosols diluted with culture medium. 24 h after treatment, MTT solution was added for 2 h, after which MTT medium was removed and the purple formazan product was extracted using 200 µL of DMSO. 100 µL of cell extract from each treatment group were transferred to a clean 96-well plate in duplicates, and absorbance was read at 570 nm with a Synergy HTX Microplate Reader (Bio Tek, VT).

For ALI exposures, 2 mL of MTT concentrate was prepared in 10 mL of BEGM medium prior to use. Apical surfaces of the transwells were rinsed with PBS. 720 mL of BEGM medium with MTT were added to the basal layer of each transwell. Cells were incubated at 37^{o} C/5% CO_2 for 2 h, after which MTT medium was removed, and the purple formazan product was extracted by adding 300 µL of DMSO to the apical layer and the absorbance was read as described above

Live cell imaging of menthol-treated cells

BEAS-2B cells in 24-well plates (8,000 cells/well) were incubated at 37°C for 24 h. Cells were treated with 0.02 or 0.2 mg/mL of menthol solution or menthol aerosol fluid and incubated in a Nikon BioStation CT (Nikon, Melville, New York). Time-lapse images were captured every 2 h for 48 h. One set of cells was plated for 24 h (attached) before treatment, while the other set (attaching) was plated simultaneously with treatment. Menthol concentrations were chosen that did not produce an effect in the MTT assay. Data were collected from five different fields in each well. Images were segmented and analyzed using CL Quant software (DR Vision) to determine the rate of growth and morphology of the control and treated cells. Cells were also treated with 0.4% trypan blue to determine the percentage of dead cells.

Intracellular calcium imaging

BEAS-2B cells (~6000 cells/well) were attached in 8-well Ibidi chamber slides (Ibidi, Munich, Germany) for 24 h, then transfected with GCaMP5 plasmid using DNA-In in Opti-MEM I Reduced Serum medium. 24 h after transfection, medium was replaced with fresh BEGM, and imaged in a stage top incubator using a Nikon Ellipse inverted microscope. XY positions of each cell were registered, and medium was replaced with medium containing 0.2 mg/mL menthol. Time-lapse videos were recorded before menthol treatment and 1, 2, 15 and 20 mins after treatment. In some experiments, the TRPM8 receptor antagonist (N(4-tert-butylphenyl)-4-(3-chloropyridin-2-yl)piperazine-1-carboxamide, BCTC-10 μM) was used for 20 mins before and during menthol treatment (Sabnis et al 2008). The change in fluorescence after treatment with/ without inhibitor was recorded using an Andor camera and analyzed using CL Quant software.

Mitochondrial ROS measurement

Mitochondrial superoxide was evaluated in submerged BEAS-2B cultures grown on cover-glass 8 well chamber slides for 24 h, then treated with 0.2 mg/mL of menthol solution for 4 h, followed by a PBS wash. Cells were then incubated with MitoSOX™ red for 2 mins at 37° C,

282 washed and examined with a Nikon Eclipse inverted microscope. Images were collected using
283 non-saturating exposures. Controls were handled similarly but received no menthol treatment.
284
285 **Detection of mitochondrial protein oxidation using the Mitotimer plasmid**

286 BEAS-2B cells (60,000 cells/insert) were allowed to attach for 24 h in transwell inserts
287 followed by transfection with MitoTimer plasmid (Addgene, Cambridge, MA) using DNA-In
288 transfecting reagent according to the manufacturer's instructions. The cells were incubated with
289 1 µg of plasmid DNA and 3 µl of DNA In (MTI-GlobalStem, MD) in Opti-MEM medium at 37^{o}C.
290 After 24 h, the transfecting medium was removed from the apical layer and fresh medium was
291 added to the basal layer. The transfected cells were exposed to menthol aerosol made with a
292 solution of 0.8 mg/mL of menthol in 0.8% sodium chloride solution using a VITROCELL® cloud
293 chamber. Untreated control samples remained in the incubator and negative controls were
294 exposed to only 0.8% sodium chloride. 24 h after exposure, cells were fixed on inserts using 4%
295 formaldehyde and insert membranes were transferred to glass slides and mounted using
296 Vectashield with DAPI (Vector Lab, Burlingame, CA). Images were collected using non-
297 saturating exposures on a Nikon Ellipse inverted microscope in the green (excitation/emission
298 488/518 nm) and red (excitation/emission 543/572 nm) channels.
299
300 **Western blotting**

301 24 h after menthol aerosol exposure in the VITROCELL® cloud chamber, cells in
302 transwells were lysed using RIPA buffer. To evaluate NF-κB activation, nuclear and cytoplasmic
303 fractions of cell suspensions were isolated after treatment using the Nuclear/Cytosol
304 Fractionation Kit (Thermo Fischer Scientific). Western blotting was performed as previously
305 described (Nair et al., 2014). Lysates were vortexed every 15 min for 1 h, centrifuged at 10,000
306 × g for 10 min at 4°C, quantified using the Pierce BCA assay kit (Thermo Scientific, Waltham,
307 Massachusetts). Lysates were mixed with Laemmli buffer (1:4), 20 µg of protein/gel lane were

separated using SDS gel electrophoresis (100 V for 2 h), and then transferred to a PVDF membrane (BioRad, Carlsbad, CA) by wet electroblotting. The membrane was blocked (5% milk in TBST buffer x 45 min) and incubated overnight at 4^{o}C with antibodies against TRPM8 (Abcam, Cambridge, MA), SOD2 (Cell Signaling Technology, Danvers, MA), or β-actin (Cell Signaling Technology, Danvers, MA). Membranes were washed for 30 min in TBST, incubated in secondary antibody for 2 h, then developed using immunoblot reagent (BioRad, Hercules, California) in a ChemiDoc™ Imaging Systems (BioRad, Hercules, California).

Quantification of cytokines (IL6 and IL8) in response to menthol treatment

Conditioned medium from the basal layer of transwells was collected 24 h post-exposure and stored at -80^{o} C. Proinflammatory cytokine release was determined using IL-6 and IL-8 ELISA kits according to the manufacturer's instructions (Invitrogen, Carlsbad, CA).

siRNA Interference assay

BEAS-2B cells were attached for 24 h in 12-well transwell inserts using serum free BEGM medium without antibiotics. Knockdown of TRPM8 and an iLamin control was carried out using siRNA (Sigma-Aldrich) and lipofectamine RNAiMAX according to the manufacturer's instructions. 24 h after transfection, medium was removed, and fresh medium was added to the basal layer. Transwells were exposed to menthol aerosol (0.8 mg/mL) in the VITROCELL® cloud chamber, and 24 h later, expression of proteins was analyzed using western blotting.

EC used for aerosol production

An Innokin iTaste MVP 3.0 battery with variable voltage (V) and wattage (W) with fresh unused SMOK Pyrex Aro bottom coil tanks and a resistance of 1.8 ohms and a voltage of 3 V (4.7 watts) was used to generate EC aerosols using a custom-built smoking machine. Tanks were loaded with 2 mL of lab-made refill fluid (10 mg/mL of menthol was prepared in 80%

propylene glycol and 20% distilled water) and used in a manner that avoided dry puffing. 80% PG was used to minimize the number of variables and to be consistent with some EC products that are commercially available (Peace et al 2016). Water, which is a component in EC fluids (National Academies of Sciences, Engineering, and Medicine. 2018), was included to dilute the PG and enable better performance of the EC. Each tank was primed with five puffs before cells were exposed.

Transepithelial electrical resistance (TEER) assay

Transepithelial electrical resistance (TEER) of EpiAirway tissue was measured with an EVOM2 voltohmmeter and a 12 mm EndOhm electrode chamber (World Precision Instruments, Sarasota, Fl). Apical surfaces of tissues were rinsed three times with PBS, 500 µL of TEER buffer were added to the apical layer, inserts were placed in an EVOM cup, and TEER readings were taken. The background resistance without the epithelial barrier present was subtracted from all measurements. The raw resistance (after background subtraction) was multiplied by 1.12 (surface area of insert) resulting in final values with units of $X \bullet cm^2$. TEER measurements following exposure are presented as the percentage of the pre-exposure value normalized to the control.

Biological Assays for Cultex Exposed Tissues

24 h after exposure, culture medium was collected from the basal side of each EpiAirway transwell, then stored at -80°C for later lactate dehydrogenase (LDH) and IL-6 and IL-8 secretion analysis. LDH was measured using the Pierce LDH Cytotoxicity Assay Kit (Rockford, IL). For full kill (positive control), non-treated EpiAirway inserts were incubated with 0.5% triton-X for 2.5 h. 50 µL of each sample and control were pipetted in duplicate into a 96-well plate with 50 µL of Reaction Mixture. After a 30-minute incubation, 50 µL of Stop Solution were added. Absorbance was read at 490 nm and 680 nm; the latter was subtracted as

background to give LDH activity which was computed as follows: % Cytotoxicity = (Sample activity – Clean Air Control activity) / (Full Kill Activity – Clean Air Control activity) x 100.

IL-6 and IL-8 concentrations were measured with enzyme-linked immunosorbent assays (ELISAs) using the manufacturers protocol (Bender MedSystems, Vienna, Austria; Life Technologies, Carlsbad, CA, USA). Prior to running the assays, IL-6 samples were diluted 1:2 using culture medium and IL-8 samples were diluted 1:100 using the dilution buffer supplied in the kit. Four replicate EpiAirway samples were run for each treatment/control group.

Protein Isolation and Proteome Processing of Cultex Exposed Tissues:

24 hours after Cultex exposure, transwell membranes were removed by cutting, the EpiAirway tissues were washed twice with PBS, then lysed in RIPA buffer by vortexing for 1 min every 15 min for 45 min at 4^0C. Lysates were centrifuged, and protein concentrations were determined using the BCA assay. 20 µg of protein were subjected to SDS-polyacrylamide gel electrophoresis, and gels were stained with Coomassie Brilliant Blue R-250 to ensure equal protein loading for each sample.

Lysates containing 150 µg of protein were precipitated with cold acetone (final concentration 80%) overnight at -20°C. Precipitates were centrifuged for 30 min at 14,000 rpm and the pellet was subjected to proteome analysis. Protein pellets were treated with 10 µL of trypsin solution (0.1 mg/ml stock solution in 50 mM ammonium bicarbonate supplemented with 10% acetonitrile) (Roche Life Science) overnight at 37°C. The samples were placed on a vortex mixer to keep proteins in suspension. After centrifuged, supernatants were dried down as pellets with a speedvac concentrator then re-dissolved in 20 µl 0.1% formic acid, to produce the sample that was subjected to liquid chromatography (LC)/mass spectroscopy (MS) analysis.

MudPIT was used to analyze the trypsin-treated samples. A two-dimensional nanoAcquity ultra-pressure liquid chromatograph (Waters, Milford, MA) and an Orbitrap Fusion MS (ThermoFisher Scientific, San Jose, CA) were configured to perform online 2D-nanoLC/MS/MS analysis. 2D-nanoLC was operated with a 2D-dilution method that is configured

with nanoAcquity UPLC. The two mobile phases for the first-dimension LC fractionation were 20 mM ammonium formate (pH 10) and acetonitrile. Online fractionation was achieved by 5-minute elution off a NanoEase trap column (PN# 186003682, Waters) using a stepwise-increased concentration of acetonitrile. A total of five fractions were generated with 11%, 16%, 20%, 25%, and 50% of acetonitrile. A final flushing step used 80% acetonitrile to clean up the trap column. Each fraction was then analyzed online using a second-dimension LC gradient. The second dimension nano-UPLC method was described previously (Drakakaki et al., 2012).

The Orbitrap Fusion MS method was based on a data-dependent acquisition (DDA) survey. The acquisition time was set from 1-70 min. A Nano ESI source was used with the spray voltage at 2600V, sweep gas at 0, and ion transfer tube temperature at 275^{o}C. An Orbitrap mass analyzer was used for the MS1 scan with resolution set at 60,000. MS mass range was 350-1800 m/z. The AGC target for each scan was 500,000 with maximal ion injection time set at 100 ms.

For the MS2 scan, the Orbitrap mass analyzer was used in an auto/normal mode with resolution at 30,000. Only precursor ions with intensities > 50,000 were selected for the MS2 scan. The sequence of individual MS2 scanning was from most-intense to least-intense precursor ions using a top-speed mode under time control of 4 sec. Higher energy CID (HCD) was used for fragmentation activation with 30% normalized activation energy. Quadrupole was used for precursor isolation with a 2 m/z isolation window. The MS2 mass range was set to auto/normal with the first mass set at 100 m/z. Maximal injection time was 100 ms with the AGC target set at 20,000. Ions were injected for all available parallelizable time. A 20-sec exclusion window was applied to all abundant ions to avoid repetitive MS2 scanning on the same precursor ions using 10 ppm error tolerance. Only charge states from 2 to 6 were allowed for MS2 scan. Undetermined charge states were not included. MS2 spectra were recorded in the centroid mode.

The raw MS files were processed/analyzed using the Proteome Discoverer version 2.1 (ThermoFisher Scientific, San Jose, CA). The Sequest HT search engine was used to match

MS data to the human Uniprot protein database supplemented with common contaminant proteins such as keratins. The search parameters were: trypsin with 2 missed cleavage, minimal peptide length for six amino acids, MS1 mass tolerance 20 ppm, MS2 mass tolerance 0.05 Da, Gln→pyro-Glu (N-term Q), oxidation (M), N-terminal acetylation as variable modification. Only proteins with a 1% false discovery rate (FDR) cut-off were considered in the final result.

Statistical Analysis

For submerged and VITROCELL® protocols, absorbance data for the MTT and ELISAs were normalized to the untreated control (submerged cultures) or to the incubator control, and the means and standard errors of the means (SEM) were determined using GraphPad Prism. For the MTT assays, the inhibitory concentrations at 50% (IC_{50}) and 70% (IC_{70}) values were computed with Prism (GraphPad, San Diego, California, USA) using the log inhibitor versus normalized response-variable slope with the top and bottom constraints set to 100% and 0%, respectively.

For experiments on calcium influx, fluorescence was quantified relative to the control (without menthol) using CL-Quant software. The statistical significance for these data was calculated using a 2-way analysis of variance ANOVA with Bonferroni's multiple comparison test. All time points in each treatment group (menthol without inhibitor and menthol with inhibitor) were compared.

A two-tailed t-test was used to analyze the mitochondrial ROS measurement (MitoSOX) and SOD2 expression using western blots. MitoTimer mitochondrial protein oxidation experiments, MTT and ELISAs were analyzed using a one-way ANOVA. When significance was found, menthol exposed groups were compared to the control using Dunnett's post hoc test.

For the proteomics data, cell-based assays (MTT, LDH, ELISAs and TEER), an ANOVA with Dunnett's post hoc test was used to compare the Clean Air Control (CA CN) to the other groups (PG control, and Menthol + PG). For the proteomics datasets, statistical analysis was done in a manner described in Statistics Analysis Supplemental to obtain adjusted p-values and fold changes for each significant protein. Proteins with known significant p-values and without a

given fold-change were assigned 100x and 0.01x fold changes for upregulation and downregulation, respectively.

To identify groups of proteins sharing common pathways, a list of significantly altered proteins was analyzed using DAVID (Huang et al., 2009) and the Ingenuity® Pathway Analysis (IPA®) omics analysis tool to discover networks and pathways of interest.

Data Access: The mass spectroscopy proteomics data (raw files) will be deposited into the ProteomeXchange Consortium.

RESULTS

Expression of TRPM8 Receptor

Menthol mediates signal transduction through the TRPM8 receptor, a ligand-gated cation channel with moderate to high selectivity for calcium ions (Peier et al., 2002). The expression of the TRPM8 receptor in human lung epithelial cells and lung fibroblasts was evaluated using western blotting and immunofluorescence microscopy (Figures 1A-C). Immunoreactivity of the TRPM8 receptor in BEAS-2B cells was intermediate between A549 cancer cells and human pulmonary fibroblasts (hPFs) (Figure 1A). The pattern of fluorescence was punctate and consistent with localization in the plasma membrane (Figure 1B). BEAS-2B cells treated with secondary antibody alone (negative control) had no label (Figure 1C).

Menthol Fluids and Aerosol Fluids Were Cytotoxic in Submerged Cultures

The cytotoxicity of pure menthol in culture medium (menthol fluid) and menthol aerosols dissolved in medium (hereafter referred to as aerosol fluid) were examined in submerged cultures using the MTT assay (Supplementary Figures 1A, B). Test solutions were considered cytotoxic if absorbance was reduced to < IC_{70} (reduction of 30% relative to the untreated control) according ISO protocol #10993-5 (ISO-10993-5-2009). Menthol fluids were cytotoxic in a concentration-dependent manner with the IC_{70} and IC_{50} values being 0.26 mg/mL and 0.87

mg/mL, respectively (Supplementary Figure 1A). Menthol concentrations as low as 0.93 mg/mL caused a significant reduction relative to the control ($p < 0.01$) in the fluid group. Menthol aerosol fluids were likewise cytotoxic producing an IC_{70} at 0.369 mg/mL. (Supplementary Figure 1B).

In Submerged Cultures Menthol Induced Calcium Influx in BEAS-2B Cells through Activation of TRPM8 Receptor

The effect of menthol on calcium influx was measured in BEAS-2B cells using GCaMP5, a genetically encoded calcium indicator plasmid (Ackerboom et al., 2012). BEAS-2B cells transfected with GCaMP5 were treated with 0.2 mg/mL of menthol (MTT NOAEL) and time-lapse video was collected (Figures 1D-G). Intracellular fluorescence was low prior to treatment (Figure 1D). There was a rapid increase in cytosolic calcium indicated by increased green fluorescence during the first minute of menthol treatment. Calcium was initially high in the perinuclear region (Figure 1E) and later became concentrated in large vesicles that were highly fluorescent (Figure 1F, Supplementary Video 1). These vesicles bulged from the surface of the cells but were not exocytosed. Pretreatment of cells with 10 μM BCTC (a TRPM8 receptor antagonist) prior to menthol treatment attenuated calcium influx caused by menthol (Figures. 1 H-K). Time-lapse data were quantified, and significant differences were seen between the menthol treated group and the BCTC group (Figure 1L). These data indicate that menthol caused calcium influx by activation of the TRPM8 receptor and not non-specific disruption of the cell plasma membrane.

Menthol Treatment Inhibited Cell Proliferation in Submerged Cultures

Live cell imaging and video bioinformatics software were used to investigate the effect of menthol fluid and menthol aerosol fluid on cell morphology, proliferation, and survival (Figure 2). BEAS-2B cells were treated with either 0.02 mg/mL (low) or 0.2 mg/mL (high) concentrations of menthol fluid or menthol aerosol fluid. Treatments were done either during plating of cells (attaching) (Figures 2 A-J) or after cells had been plated and attached for 24 h (Figures 2K-T).

The low concentration of both menthol fluid and aerosol fluid did not affect proliferation of attaching cells (Figures 2D, H, and U). However, when attaching BEAS-2B cells were treated with the high concentration of menthol fluid during plating, they did not proliferate (Figure 2F). In contrast, the high concentration (0.2 mg/mL) of menthol aerosol fluid did not affect proliferation of attaching cells (Figure 2J), probably because not all menthol transferred to the aerosol fluid.

When attached BEAS-2B cells were treated with the high concentration (0.2 mg/mL) of menthol fluid or menthol aerosol fluid, proliferation was significantly decreased (Figures 2P,T and V), while the low concentration of aerosol fluid had an effect intermediate between the high concentration and the untreated controls (Figures 2R and V). The low concentration of fluid did not affect attached cells (Figure 2N).

ROS Generation in Submerged Cultures

To investigate effects downstream of menthol-induced calcium elevation, intracellular ROS was measured in menthol fluid-exposed BEAS-2B cells in submerged culture. Superoxide ($O_2^{\bullet-}$) generated from mitochondrial oxidative phosphorylation is a major source of cellular ROS. MitoSOX Red, a fluorescent indicator specific for superoxide, was used to localize and quantify superoxide in menthol-treated cells. Live cell imaging results for BEAS-2B cells incubated with MitoSOX showed increased mitochondrial ROS generation in menthol fluid (0.2 mg/mL, MTT NOAEL) treated cells (Figures. 3A, B). Menthol induced mitochondrial ROS was decreased when cells were pretreated with BCTC prior to menthol exposure (Figures. 3C, D). Rotenone (500nM) was used as a positive control and produced results similar to Figure 3A Menthol (Supplement Figure 1C).

Oxidative Stress Occurs During ALI Exposure of BEAS-2B Monolayers to Unheated Menthol Aerosol Generated Using a Cloud Chamber

A VITROCELL® cloud chamber was used to determine how monolayers of BEAS-2B cells respond when exposed to menthol at the air-liquid interface (ALI). The cloud chamber

creates an aerosol without heating, without use of a solvent such as PG, and without introduction of heat-induced reaction products. It therefore allows pure menthol to be studied without co-constituents. Menthol (0.8 mg/mL) aerosol was generated in the cloud chamber as described in Materials and Methods. The actual concentration of menthol in the aerosol in both the VITROCELL® and Cultex experiments was not directly measured, but 100% transfer was assumed. The MTT assay indicated that cytotoxicity (absorbance < 70% of the control) was not induced by menthol in BEAS-2B cells using our exposure protocol in the VITROCELL® cloud chamber (Figure 4A).

To visualize mitochondria and oxidation of mitochondrial proteins, we transfected cells with the MitoTimer plasmid, which is targeted to mitochondria via cytochrome c (Laker et al., 2014). MitoTimer fluoresces green when mitochondrial protein is not oxidized. As protein oxidation increases, the fluorescence shifts from green to red. Cells transfected with the MitoTimer plasmid were exposed to menthol aerosol (0.8 mg/mL) in the VITROCELL® cloud chamber as described in the Materials and Methods. Ratiometric analysis of red/green MitoTimer fluorescence revealed a statistically significant increase of mitochondrial protein oxidation in menthol treated cells (Figures 4B, C). A change in mitochondrial morphology was also observed in treated cells (Figure 4B). Mitochondria were predominantly networked in control cells (Figure 4B1, *2, 3,* 4) and punctate after menthol treatment (Figure 4B: Micrographs 5, 6, 7, and 8)

Cellular ROS levels are regulated by antioxidant systems. The most crucial antioxidant is manganese superoxide dismutase (MnSOD/SOD-2), which neutralizes superoxide by converting it into hydrogen peroxide (H_2O_2) (Holley et al., 2011). Aerosol generated using 0.8 mg/mL of menthol increased expression of SOD2 in a concentration dependent manner, as shown in western blots (Figures 4D, F). We next investigated the effect of TRPM8 silencing on SOD2 expression. Knockdown of TRPM8 using siRNA prior to menthol exposure significantly reversed the effect of menthol aerosol on SOD2 levels in treated cells (Figures 4 E, G).

Activation of Nuclear Factor Kappa B (NF-κB) is Stimulated by ALI Exposure to Unheated Menthol Aerosol Generated Using a Cloud Chamber

NF-κB is a transcription factor that is activated in response to several stimuli, including oxidative stress. To evaluate the role of menthol in NF-κB activation, cells were exposed to menthol aerosol (0.8 mg/mL) in a VITROCELL® cloud chamber as described in the Materials and Methods. 24 h after menthol aerosol exposure, there was a significant increase in phospho-NF-κB (active form) expression in the whole cell lysate when compared to the untreated control (Figure 5A). To assess the translocation of phospho-NF-κB into the nucleus, cells treated with or without menthol aerosol were subjected to cell fractionation to separate nuclear and cytoplasmic proteins. There was a significant increase in phospho-NF-κB in the nuclear fraction of cells exposed to menthol aerosol (Figure 5B).

Secretion of Inflammatory Cytokines (IL6 and IL8) is Stimulated by ALI Exposure to Unheated Menthol Aerosol Generated Using a Cloud Chamber

IL-6 and IL-8 are cytokines that are up-regulated in inflamed airways and airways of asthma patients (Rincon and Irvin, 2012). The effect of menthol aerosol on secretion of IL6 and IL8 was evaluated following ALI exposure of monolayers of BEAS-2B cells to menthol aerosol in a VITROCELL® cloud chamber. 24 h after exposure, conditioned medium was collected from the inserts, and Day 1 cytokine secretion was analyzed using an ELISA. Fresh medium was added to each insert, and this was collected and analyzed after an additional 24 h of incubation (Day 2). ALI exposure of BEAS-2B cells to unheated menthol aerosol caused an elevation of IL6 and IL8 secretion (Figures 5C, D). Menthol increased the secretion of IL6 and IL8 at least two-fold compared to the control after 24 and 48 h of incubation period.

Cytotoxic, TEER, and Proteomic Effects of ALI Exposure of EpiAirway Tissue to Heated Menthol Aerosol Produced in an EC

Experiments were performed using 3D EpiAirway tissues to determine if similar effects on oxidative stress and inflammatory cytokine elevation occurred following ALI exposure to menthol-containing aerosols created with an EC. In this protocol, the aerosol was heated and therefore contained, in addition to menthol, solvent (PG) and any reaction products generated by heating. Endpoints included cytotoxicity (MTT assay), TEER measurements, ELISAs, and proteomics analysis of cells following exposure.

EpiAirway tissues were exposed at the ALI to 30 puffs of aerosol produced with an EC at relatively low voltage/power (3V/ 5 watts) then allowed to recover for 24 hours before evaluation with the TEER (Supplementary Figure 2A) and cytotoxicity assays (MTT, LDH) (Supplementary Figure 2B, C). Apart from a small decrease in TEER in the PG control group, tissue integrity was not affected by menthol aerosol treatment when compared to the clean air control (Supplementary Figure 2A). There was no significant effect on mitochondrial reductase activity (Supplementary Figure 2B) in the treatment or PG group. In the LDH assay, there was no effect in the PG control group, and a small decrease in the menthol group (Supplementary Figure 2C), which, although statistically significant, may not be biologically relevant.

To determine the effect of menthol aerosol exposures on the proteome of EpiAirway tissue, protein samples were harvested 24 hours after exposure to clean air (CA), PG vehicle control, or menthol. A mass spectrometry (MS) bottom up proteomics method with the False Discovery Rate (FDR) controlled at 1% was performed, which identified 4,462 unique proteins in menthol treated cells (Figures 6A). An in-house statistical method identified 192 significant proteins (35 downregulated and 157 upregulated) in the menthol group and the 22 significant proteins (11 downregulated and 11 upregulated) in the PG group that had differential abundance relative to clean air (Figures 6B, D). Our stringent statistical model was developed (Statistics Analysis Supplemental) to isolate the effect of menthol aerosols from the PG vehicle, resulting in the unconventional shape of the volcano plots (Figures 6B, C). Despite the efforts to exclude PG from the analysis, PG still showed an effect on protein expression (Figure 6C, B),

593 which is consistent with recent reports of PG toxicity and respiratory irritation (Behar et al.,
594 2017; Ghosh et al., 2018)

595 **Protein Pathway Interactome Analysis using DAVID**

596 Menthol and PG aerosol exposure data were analyzed using DAVID to show the
597 pathway clusters affected by each treatment group (Fig. 7, Purple circle: PG, Green circle:
598 Menthol). Menthol aerosol treated cells expressed proteins related to xenobiotic stress,
599 oxidative stress, and inflammation among others, including cytoskeletal activity. Mitochondrial
600 pathway clusters were affected both by menthol and PG aerosols.

601 **Cell Signaling Pathways Affected by Menthol Aerosol Exposure using IPA**

602 IPA pathway enrichment analysis was used to identify canonical pathways significantly
603 impacted by menthol aerosol exposure (Figure 8A). A positive z-score (>2) represents an
604 increase in a cellular process, while a negative z-score (<-2) indicates a decrease. Enrichment
605 of proteins related to oxidative stress (NRF2 mediated oxidative stress response, EIF2
606 signaling), inflammatory cytokine signaling (IL8 signaling), metabolic pathways (oxidative
607 phosphorylation and gluconeogenesis) among other pathways were found. Top pathways
608 included oxidative phosphorylation (which could increase oxidative stress) and NRF-2 mediated
609 oxidative stress response. Upregulation of EIF2 signaling was verified using western blotting
610 (Supplemental Figure 3A, B). In addition, pathways related to cell proliferation regulation
611 (HIPPO signaling, PTEN signaling, and Cyclins and Cell Cycle Regulation) were downregulated.
612 Chemokine secretion of IL6 and IL8 was investigated using ELISAs and found to be increased
613 significantly in treatment groups relative to clean air controls (Supplemental Figure 4A, B).

614 Proteins uploaded into IPA (Ingenuity Pathway Analysis) for the menthol group were
615 annotated with associations to various cellular processes. 51.02% of the proteins (N=50) were
616 affiliated with general cellular response, 29% (N=14) with gene expression regulation, 29%

(N=14) with immune response, 27% (N=13) with cancer, and 7.14% (N=7) with metabolism pathways (Figure 8B).

DISCUSSION

This is the first study to compare the toxic effects of MTT NOAEL concentrations of menthol on human respiratory epithelium using submerged cultures and ALI exposures with and without solvents and with and without heating the aerosols. In most assays, there was excellent agreement of results across the three *in vitro* platforms. At menthol concentrations that did not produce an effect in the MTT assay, oxidative stress was observed with all three platforms, and cytokine elevation/secretion was found in both ALI exposure protocols. These data show that screening toxicants using BEAS-2B cells in 2D submerged cultures or in cloud chamber ALI exposures provides reliable data that could subsequently be confirmed in the more expensive and labor-intensive 3D ALI EpiAirway model. Our data also support the use of submerged cultures for assays that are difficult to perform in 3D ALI exposures, such as monitoring calcium influx through the TRPM8 receptor and live cell imaging.

Menthol induced cytotoxicity in BEAS-2B cells was concentration-dependent (submerged culture protocol). Cytotoxicity (MTT assay) was not observed in the VITROCELL® and Cultex system, probably because exposures were relatively short compared to 24 hours of continual exposure in submerged cultures. In the live cell imaging experiment (submerged culture), the ability of attaching cells to better withstand menthol treatment may be due to removal of cell surface proteins (including TRPM8) by trypsin during detachment of cells for plating (Zhang et al., 2012). Attached cells likely regenerated TRPM8 during the 24-h attachment period before treatment and thus were immediately affected when exposed to menthol. The increased toxicity observed in menthol aerosol fluids during live cell imaging could be due to reaction products, such as formaldehyde, acrolein, and acetaldehyde (Kosmider et al., 2014), that formed from menthol and/or propylene glycol during heating (Behar et al., 2018). In

addition, variations in proliferation of attaching vs attached cells in submerged culture show that certain cellular responses can vary within exposure protocols and that cell proliferation is more sensitive to protocol variation than oxidative stress and inflammation. The 3D EpiAirway (Cultex) data on cell proliferation were inconclusive. Some pathways (downregulation of PTEN signaling, downregulation of HIPPO signaling) suggest an increase in cell proliferation, while others (upregulation of CHK, downregulation of cyclins and cell cycle regulation) suggest a decrease (Halder and Johnson, 2011; Jiang and Liu, 2009; Harvey et al., 2013; Stacey, 2003; Wu et al., 2003; Xiao et al., 2006).

We detected the TRPM8 receptor in BEAS-2B cells, A549 cells, and hPFs with relatively more expression in the lung cancer cells (A549). Osteosarcoma, pancreatic, and breast cancer cells also have elevated levels of TRPM8, where it may function in the development and progression of tumors (Liu et al., 2016; Yee, 2015; Zhao et al., 2018). In our immunolabeling data, TRPM8 was localized to the plasma membrane, while another report found it in both the plasma membrane and rough endoplasmic reticulum (ER) (Sabnis et al., 2008). The differences in labeling may be related to the use of different antibodies (polyclonal versus monoclonal). In lung cells, TRPM8 is thought to detect cold temperatures (Bautista et al., 2007), while a less recognized function may be to respond to inhaled chemicals, such as menthol, and activate stress/survival responses.

Our data show that the TRPM8 receptor is functional in BEAS-2B cells. In submerged culture, the initiating event during menthol exposure was a rapid influx of calcium through the TRPM8 receptor, which was inhibited by BCTC. This observation agrees with a previous study in which a higher concentration of menthol (2.5 mM vs 1.3 mM in the current study) induced calcium influx into BEAS-2B cells (Sabnis et al., 2008). Our data showed a rapid increase first in cytosolic calcium (Fig. 1E), suggesting initial influx through the plasma membrane, followed by increased fluorescence in vesicles that are likely of ER origin (Fig.1 F). These vesicles moved adjacent to, but did not fuse with, the plasma membrane, suggesting they quickly sequester

669 excess cytosolic calcium and pump it out near calcium exporters at the cell surface (e.g., Ca^{2+}-
670 ATPase and $Na+/Ca^{2+}$ exchanger) (Guerini et al., 2005). The TRPM8 receptor has been
671 reported in the ER (Sabnis et al., 2008). Because the TRPM8 receptor would have opposite
672 orientations in the plasma and ER membranes, it is possible TRPM8 in the ER is also activated
673 by menthol and facilitates removal of excess calcium from the cell.

674 In submerged cultures, menthol also increased mitochondrial ROS in BEAS-2B cells,
675 which was likely due to the increase in intracellular calcium. Elevation of cytosolic calcium can
676 cause a rise in mitochondrial calcium through the mitochondrial uniporter channel (MCU)
677 (Rizzuto et al., 2000; Samanta et al., 2014), and excess calcium in mitochondria can enhance
678 ROS generation (Brookes et al., 2004)

679 In the VITROCELL® cloud chamber, oxidative stress and an inflammatory response
680 occurred during exposure to relatively low concentrations of menthol (0.8 mg/mL), which did not
681 produce an effect in the cloud chamber MTT assay. The cloud chamber enabled pure menthol-
682 containing aerosol to be tested without solvents (PG or glycerin) and without heat-generated
683 reaction-products, which distinguishes this protocol from prior ALI studies with EC flavor
684 chemicals (Azzopardi et al., 2016; Leigh et al., 2018). BEAS-2B cells exposed to menthol at the
685 ALI showed an increase in oxidation of mitochondrial proteins and the mitochondrial specific
686 antioxidant enzyme SOD2, both signs of oxidative stress not previously reported for cells
687 treated with menthol at the ALI (Muthumalage et al., 2018; Zhao and Xu, 2016; Zhao et al.,
688 2018). Because these effects were observed in the cloud chamber, they can be attributed to
689 menthol *per se* and not solvents or heat-generated reaction products. Menthol also increased
690 the number of punctate mitochondria, a sign of stress that could lead to mitophagy (Tondera et
691 al., 2009; Zahedi et al., 2018). A similar increase in punctate mitochondria was observed in
692 BEAS-2B and A549 cells treated with rotenone or antimycin, and was attributed to calcium influx
693 into the mitochondria and increased ROS generation (Ahmad et al., 2013). Increased ROS and
694 oxidation of mitochondrial protein also occurred following exposure of neural stem cells to

695 thirdhand cigarette smoke or electronic cigarette aerosol fluids (Bahl et al., 2016; Zahedi et al.,
696 2018). SOD2, which is located in mitochondria, is a major ROS detoxifying enzyme (Holley et
697 al., 2011). The elevation of SOD2 in BEAS-2B cells exposed to menthol aerosol was inhibited
698 by siRNA knock down of the TRPM8 receptor, supporting the conclusion that menthol-induced
699 oxidative stress occurred through activation of this receptor.

700 In the Cultex protocol, 3D EpiAirway tissue was exposed to aerosol containing pure
701 menthol, PG, and heat-generated reaction products that formed in an EC. This aerosol is
702 equivalent to that inhaled by an EC user. Proteins involved in oxidative stress (e.g., oxidative
703 phosphorylation proteins and NRF-2 mediated oxidative stress) and in inflammatory response
704 (e.g., IL-8 signaling) were elevated in the Cultex mentho-treated group, consistent with data
705 obtained with the other two exposure protocols. IL-8 signaling, which was causally linked to
706 acute inflammation (Harada et al., 1994), was the second most upregulated pathway in our
707 Cultex data. While the VITROCELL® cloud chamber data clearly show that menthol can elevate
708 IL8 secretion, the Cultex data further show that PG is also effective, despite efforts to
709 statistically remove its influence from the proteomics analysis. PG is therefore a health concern
710 (Callahan-lyon, 2014; Wieslander et al., 2001) due to its ubiquitous use in EC products will be
711 evaluated in more depth in a future study.

712 In addition to corroborating data obtained with submerged cultures and the cloud
713 chamber, the proteomics analysis of Cultex data identified other pathways that were significantly
714 affected in menthol exposed cells. As examples, NGF signaling, which was increased in the IPA
715 analysis, is involved in activation of NF-κB, a protein that was detected in the DAVID cluster
716 analysis (Figure 7A, 8). NF-kB is normally present in inactive form in cells allowing it to become
717 rapidly activated upon exposure to harmful stimuli (Perkins and Gilmore, 2006). Experiments
718 with tobacco cigarette users and dual users (EC plus and cigarettes) showed upregulation of
719 NGF signaling, glutathione transferase, and NRF2 signaling (D'Anna et al., 2015; Ghosh et al.,
720 2018), suggesting that ECs and conventional cigarettes have similar xenobiotic effects. In

addition, Rho family GTPase signaling, Rac signaling, and integrin signaling are pathways that affect the cytoskeleton (Symons, 1996). Their upregulation may have been involved in formation of the calcium-rich blebs seen in submerged cultures. Blebbing involving these proteins/pathways occurs in response to calcium influx in human embryonic stem cells upon activation of the P2X7 receptor, which causes rapid influx of calcium (Guan et al., 2016; Weng et al., 2018; Weng and Talbot, 2017).

Our data support the idea that menthol, at concentrations found in EC aerosols, can disturb cell homeostasis and with chronic exposure may contribute to respiratory diseases. Elevation of ROS is involved in numerous diseases, including chronic inflammation (Saito et al., 2006; Takeda et al., 1999; Teramoto et al., 1999). One of the main signaling pathway/transcription factors triggered by oxidative stress is NF-κB (Perkins and Gilmore, 2006). In humans, the bronchiolar epithelium is an important site for NF-κB activation and expression of NF-κB dependent inflammatory mediators (Poynter et al., 2002). NF-κB targets genes that attenuate ROS to promote survival (Djavaheri-Mergny et al., 2004; Kairisalo et al., 2007) and regulates expression of the immunomodulatory cytokines. Elevated NF-kB and induced secretion of two proinflammatory cytokines (IL6 and IL8) are commonly seen in inflammatory pulmonary diseases (Rincon and Irvin, 2012). Acute and chronic inflammation play roles in the pathogenesis of lung disorders, such as asthma, COPD, adult respiratory distress syndrome, and idiopathic pulmonary fibrosis (Cheng et al., 2007). Although menthol was not established as the causative agent, chronic inflammation from the use of tobacco cigarettes has been linked with Acute Respiratory Distress Syndrome (ARDS) and COPD (Cantin, 2010; Miller et al., 1992; Vaart et al., 2013).

Menthol is present in some mint-flavored EC refill fluids at 84 mg/mL (Behar et al., 2018), which is well above 1 mg/mL, which produced a strong cytotoxic effect in the MTT assay (submerged culture) (Supplemental Fig. 1). Consideration should be given to the possibility that the high concentrations of flavor chemicals in some EC products (Omaiye et al., 2019), such as

menthol at 84 mg/mL, could kill the respiratory epithelium resulting in the “burn” characteristics described by some physicians treating EVALI patients (Butt et al., 2019). The dangers of inhaling high concentrations of menthol are further supported by a case report in which acute menthol inhalation caused the death of an other-wise healthy factory worker cleaning a peppermint storage vat; after inhaling menthol fumes for several hours, the 21 year old worker became unconscious, did not respond to treatment, and died 14 days later (Kumar et al., 2016).

The Center for Disease Control (CDC) reports 2,807 EVALI cases and 68 deaths related to EC usage (Centers for Disease Control and Prevention, 2019). While awaiting firm regulations on the use of flavor chemicals in ECs, the FDA issued a guidance for industry in January 2020 that prohibits the use of flavor chemicals, but excluded both tobacco and menthol flavors (Food and Drug Administration Center for Tobacco Products, 2020), potentially leaving public health susceptible to adverse effects from chronic use of menthol at concentrations reported in this study or from acute harm by products with high concentrations of menthol.

Conclusions

The three *in vitro* platforms for exposing respiratory epithelium to menthol each lead to similar conclusions. Concentrations of menthol within the range found in many EC fluids and aerosols produced rapid calcium influx followed by an increase in oxidative stress and inflammatory cytokines. These responses were inhibited by BCTC and siRNA knock-down of the TRPM8 receptor. Taken together, these data provide a strategy for evaluating the toxicity of inhaled chemicals by first screening in the MTT assay to identify cytotoxic concentrations and possible modes of action. Authentic standards can next be tested at the ALI first using cloud chamber exposure to avoid solvents and reaction products formed by heating, followed by exposure to authentic EC aerosol as done in the Cultex. Using proteomics with ALI exposure systems has the advantage of both confirming and discovering pathways simultaneously. In future studies, it will be valuable to show effects similar to those observed with the EpiAirway

protocol in EC users. Validation of the EpiAirway model for translation to *in vivo* exposure would be valuable and could replace animal testing, reduce experimental costs, and accelerate research progress. Data obtained with this approach support the conclusion that menthol, at concentrations found in EC aerosols, adversely affects bronchial epithelial cells, which could disrupt tissue homeostasis, impair cell function, and lead to disease, including some of the recently reported cases of EVALI.

Limitations of the Study

The effects of menthol were analyzed with exposure to relatively low EC doses. Increasing the number of puffs or voltage of ECs could increase the toxicity of menthol aerosols. In another Cultex study, 200 puffs of aerosol delivered over about 30 min caused differences in cell viability depending on the cell type used (Scheffler et al., 2015). Therefore, results with ALI exposure will vary depending on the protocol. Because of the large variability in EC puffing topography (Behar et al., 2015), it would be useful to develop at least two standard protocols for both the high and low.

ACKNOWLEDGEMENTS

Research reported in this publication was supported by NIDA, NIEHS, and the FDA Center for Tobacco Products (CTP) grant #s R01DA036493 and R01ES029741. The content is solely the responsibility of the authors and does not necessarily represent the official views of the NIH or the Food and Drug Administration. The Orbitrap Fusion mass spectrometer was purchased with funds from an NIH shared instrumentation grant (S10OD010669). We thank Lindsey Bustos for her help with the VITROCELL® exposures as well as Man Wong for his helpful remarks.

AUTHOR CONTRIBUTIONS

Project administration and funding acquisition, P.T and JFP.; Conceptualization, V. N. and P.T.; Investigation, V. N., M T, R.B, Y.W, R.P., W. L and, proteomics analysis, V. N., M. T., S. P., Proteomics statistical analysis, S.Z. and X. C.; Writing, all authors.

DECLARATION OF INTERESTS

The authors have no competing interests to declare.

References

Akerboom, J., Chen, T.-W., Wardill, T.J., Tian, L., Marvin, J.S., Mutlu, S., Calderon, N.C., Esposti, F., Borghuis, B.G., Sun, X.R., et al. (2012). Optimization of a GCaMP calcium indicator for neural activity imaging. J Neurosci. 2012 Oct 3;32(40):13819-40. DOI: 10.1523/JNEUROSCI.2601- 12.2012

Ahmad, T., Aggarwal, K., Pattnaik, B., Mukherjee, S., Sethi, T., Tiwari, B.K., Kumar, M., Micheal, A., Mabalirajan, U., Ghosh, B., Roy, S.S., Agrawal, A., (2013). Computational classification of mitochondrial shapes reflects stress and redox state. Cell Death Dis. 2013 Jan 17;4: e461. DOI: 10.1038/cddis.2012.213

Ai, J., Taylor, K.M., Lisko, J.G., Tran, H., Watson, C.H., Holman, M.R., (2016). Original investigation menthol content in US marketed cigarettes. Nicotine Tob Res. 2016 Jul;18(7):1575-80. https://doi.org/10.1093/ntr/ntv162

Azzopardi, D., Patel, K., Jaunky, T., Santopietro, S., Camacho, O.M., Mcaughey, J., Gaça, M., (2016). Electronic cigarette aerosol induces significantly less cytotoxicity than tobacco smoke. Toxicol Mech Methods. 2016 Jul;26(6):477-491. DOI: 10.1080/15376516.2016.1217112

Bahl, V., Johnson, K., Phandthong, R., Zahedi, A., Schick, S.F., Talbot, P., (2016). Thirdhand cigarette smoke causes stress-induced mitochondrial hyperfusion and alters the transcriptional profile of stem cells. Toxicol Sci. 2016 Sep;153(1):55-69. DOI: 10.1093/toxsci/kfw102

Bahl, V., Lin, S., Xu, N., Davis, B., Wang, Y., Talbot, P., Oak, R., (2012). Comparison of electronic cigarette refill fluid cytotoxicity using embryonic and adult models. Reprod Toxicol. 2012 Dec;34(4):529-37. DOI: 10.1016/j.reprotox.2012.08.001

Barrington-Trimis, J.L., Leventhal, A., (2018). Adolescents' use of "pod mod" e-cigarettes - urgent concerns. N Engl J Med. 2018 Sep 20;379(12):1099-1102. DOI: 10.1056/NEJMp1805758

Bautista, D.M., Siemens, J., Glazer, J.M., Tsuruda, P.R., Basbaum, A.I., Stucky, C.L., Jordt, S., Julius, D., (2007). The menthol receptor TRPM8 is the principal detector of environmental cold. Nature. 2007 Jul 12;448(7150):204-8. DOI: 10.1038/nature05910

Behar, R.Z., Davis, B., Wang, Y., Bahl, V., Lin, S., Talbot, P., (2014). Identification of toxicants in cinnamon-flavored electronic cigarette refill fluids. Toxicol. Vitro 2014 March;(28): 198–208. DOI: https://doi.org/10.1016/j.tiv.2013.10.006

Behar, R.Z., Hua, M., Talbot, P., (2015). Puffing topography and nicotine intake of electronic cigarette users. PLoS One. 2015 Feb 9;10(2):e0117222. DOI:10.1371/journal.pone.0117222

Behar, R.Z., Luo, W., Lin, S.C., Wang, Y., Valle, J., Pankow, J.F., Talbot, P., (2016). Distribution, quantification and toxicity of cinnamaldehyde in electronic cigarette refill fluids and aerosols. Tob Control. 2016 Sep 15;25: ii94–ii102. DOI: 10.1136/tobaccocontrol-2016-053224

Behar, R.Z., Luo, W., Mcwhirter, K.J., Pankow, J.F., Talbot, P., (2018). Analytical and toxicological evaluation of flavor chemicals in electronic cigarette refill fluids. Scientific Reports volume 8, Article number: 8288 (2018). DOI: 10.1038/s41598-018-25575-6

Behar, R.Z., Wang, Y., Talbot, P., (2017). Comparing the cytotoxicity of electronic cigarette fluids, aerosols and solvents. Tob Control. 2018 May;27(3):325-333. DOI: 10.1136/tobaccocontrol-2016-053472

Brookes, P.S., Yoon, Y., Robotham, J.L., Anders, M.W., Sheu, S., (2004). Calcium, ATP, and ROS: a mitochondrial love-hate triangle. Am J Physiol Cell Physiol. 2004 Oct;287(4):C817-33. DOI: 10.1152/ajpcell.00139.2004

Butt, Y.M., Smith, M.L., Tazelaar, H.D., Vaszar, L.T., Swanson, K.L., Cecchini, M.J., Boland, J.M., Bois, M.C., Boyum, J.H., Froemming, A.T., Khoor, A., Mira-Avendano, I., Patel, A., Larsen, B.T., (2019). Pathology of Vaping-Associated Lung Injury. N Engl J Med 2019; 381:1780-1781. DOI: 10.1056/NEJMc1913069

Callahan-lyon, P., (2014). Electronic cigarettes: human health effects. Tobacco control 23 Suppl 2(Suppl 2): ii36-ii40 · May 2014. http://dx.doi.org/10.1136/tobaccocontrol-2013-051470

Cantin, A.M., (2010). Cellular response to cigarette smoke and oxidants: adapting to survive. Proc Am Thorac Soc. 2010 Nov;7(6):368-75. DOI: 10.1513/pats.201001-014AW

Center for Disease Control and Prevention, (2019). States update number of hospitalized EVALI cases and EVALI deaths. Retrieved from https://www.cdc.gov/media/releases/2019/s1231-evali-cases-update.html

Cheng, D., Han, W., Chen, S.M., Taylor, P., Chont, M., Park, G., Sheller, J.R., Polosukhin, V. V, Christman, J.W., Yull, F.E., Blackwell, T.S., Cheng, D., Han, W., Chen, S.M., Sherrill, T.P., Chont, M., Park, G., Sheller, J.R., Polosukhin, V. V, Christman, J.W., Yull, F.E., Blackwell, T.S., (2007). Through the NF- κB pathway 1. J Immunol May 15, 2007, 178 (10) 6504- 6513. DOI: https://doi.org/10.4049/jimmunol.178.10.6504

D'Anna, C., Cigna, D., Costanzo, G., Bruno, A., Ferraro, M., Vincenzo, D., Bianchi, L., Bini, L., Pace, E., (2015). Cigarette smoke alters the proteomic profile of lung fibroblasts. Mol Biosyst. 2015 Jun;11(6):1644-52. DOI: 10.1039/c5mb00188a

Delnevo, C.D., Gundersen, D.A., Hrywna, M., Echeverria, S.E., Steinberg, M.B., (2011). Smoking-cessation prevalence among U.S. smokers of menthol versus non-menthol cigarettes. Am J Prev Med. 2011 Oct;41(4):357-65. DOI: 10.1016/j.amepre.2011.06.039

DeVito, E.E., Jensen, K.P., O'Malley, S.S., Gueorguieva, R., Krishnan-Sarin, S., Valentine, G., Jatlow, P.I., Sofuoglu, M., (2019). Modulation of "protective" nicotine perception and use profile by flavorants: preliminary findings in e-cigarettes. Nicotine Tob Res. 2019 Apr 17. pii: ntz057. DOI: 10.1093/ntr/ntz057

Djavaheri-Mergny, M., Javelaud, D., Wietzerbin, J., Besancon, F., (2004). NF- κB activation prevents apoptotic oxidative stress via an increase of both thioredoxin and MnSOD levels in TNFα-treated Ewing sarcoma cells. FEBS Lett. 2004 Nov 11;578(1-2): 111–115. DOI: https://doi.org/10.1016/j.febslet.2004.10.082

Drakakaki, G., Van De Ven, W., Pan, S., Miao, Y., Wang, J., Keinath, N.F., Weatherly, B., Jiang, L., Schumacher, K., Hicks, G., Raikhel, N., (2012). Isolation and proteomic analysis of the SYP61 compartment reveal its role in exocytic trafficking in Arabidopsis. Cell Res. 2012 Feb;22: 413–424. DOI: 10.1038/cr.2011.129

Ending new nicotine dependencies act of 2019 (ENND Act), S.2519, 116th cong. (2019-2020).

Family Smoking Prevention and Tobacco Control Act of 2009, 5 USC §§ 1776-1858 (2009).

Food and Drug Administration, (2011). Preliminary scientific evaluation of the possible public health effects of menthol versus nonmenthol cigarettes. Retrieved from https://permanent.access.gpo.gov/gpo39032/Preliminary%20Scientific%20Evaluation%20Menthol%20508%20reduced.pdf

Food and Drug Administration, Center for Tobacco Products, (2020). Enforcement Priorities for Electronic Nicotine Delivery Systems (ENDS) and Other Deemed Products on the Market Without Premarket Authorization. Retrieved from: https://www.fda.gov/regulatory-information/search-fda-guidance-documents/enforcement-priorities-electronic-nicotine-delivery-system-ends-and-other-deemed-products-market

Ghosh, A., Coakley, R.C., Mascenik, T., Rowell, T.R., Davis, E.S., Rogers, K., Webster, M.J., Dang, H., Herring, L.E., Sassano, M.F., Livraghi-butrico, A., Buren, S.K. Van, Graves, L.M., Herman, M.A., Randell, S.H., Alexis, N.E., Tarran, R., Carolina, N., (2018). Chronic e-cigarette exposure alters the human bronchial epithelial proteome. Am J Respir Crit Care Med. 2018 Jul 1;198(1):67-76. DOI: 10.1164/rccm.201710-2033OC

Grady, D., (2019, Nov 8). Lung damage from vaping resembles chemical burns, report says. The New York Times

Guan, B.X., Bhanu, B., Talbot, P., Weng, N.J., (2016). Extraction of blebs in human embryonic stem cell videos. IEEE/ACM Trans Comput Biol Bioinform. 2016 Jul-Aug;13(4):678-88. DOI: 10.1109/TCBB.2015.2480091

Guerini, D., Coletto, L., Carafoli, E., (2005) Exporting calcium from cells. Cell Calcium 38: 281-289.

Halder, G., Johnson, R.L., (2011). Hippo signaling: growth control and beyond. Development. 2011 Jan;138(1):9-22. DOI: 10.1242/dev.045500

Hallagan, J., (2014). The safety assessment and regulatory authority to use flavors: focus on e-cigarettes. Retrieved from: https://www.femaflavor.org/node/24344

Harada, A., Sekido, N., Akahoshi, T., Wada, T., Mukaida, N., Matsushima, K., (1994). Essential involvement of interleukin-8 (IL-8) in acute inflammation. J Leukoc Biol. 1994 Nov;56(5):559-64. https://doi.org/10.1002/jlb.56.5.559

Harvey, K.F., Zhang, X., Thomas, D.M., (2013). The hippo pathway and human cancer. Nat Rev Cancer. 2013 Apr;13(4):246-57. DOI: 10.1038/nrc3458

Henderson, B.J., (2019). Chapter 12 - linking nicotine, menthol, and brain changes. In Neuroscience of Nicotine Mechanisms and Treatment, V. Preedy, ed. (Science Direct), pp. 87-95.

Holley, A.K., Bakthavatchalu, V., Velez-roman, J.M., Clair, D.K.S., (2011). Manganese superoxide dismutase: guardian of the powerhouse. Int J Mol Sci. 2011;12(10):7114-62. DOI: 10.3390/ijms12107114

Hua, M., Omaiye, E.E., Luo, W., Mcwhirter, K.J., Pankow, J.F., Talbot, P., (2019). Identification of cytotoxic flavor chemicals in top-selling electronic cigarette refill fluids. Scientific Reports volume 9, Article number: 2782 (2019) .DOI:10.1038/s41598-019-38978-w

961 Huang, D.W., Sherman, B.T., Lempicki, R.A., (2009). Systematic and integrative analysis of
962 large gene lists using DAVID bioinformatics resources. Nat. Protoc. 2009;4(1): 44–57. DOI:
963 10.1038/nprot.2008.211
964
965 Jiang, B., Liu, L., (2009). PI3K / PTEN signaling in tumorigenesis and angiogenesis. Adv Cancer
966 Res. 2009;102:19-65. DOI: 10.1016/S0065-230X(09)02002-8
967
968 Kairisalo, M., Korhonen, L., Blomgren, K., Lindholm, D., (2007). X-linked inhibitor of apoptosis
969 protein increases mitochondrial antioxidants through NF- κB activation. Biochem Biophys Res
970 Commun. 2007 Dec 7;364(1):138-44. DOI: 10.1016/j.bbrc.2007.09.115
971
972 Kosmider, L., Sobczak, A., Fik, M., Knysak, J., Zaciera, M., Kurek, J., Goniewicz, M.L., (2014).
973 Carbonyl compounds in electronic cigarette vapors: effects of nicotine solvent and battery
974 output voltage. Nicotine Tob Res. 2014 Oct;16(10):1319-26. DOI: 10.1093/ntr/ntu078
975
976 Kumar, A., Baitha, U., Aggarwal, P., and Jammshed, N. (2016) A fatal case of menthol
977 poisoning. Int Journal of App and Basic Med Res. 6: 137-139.
978
979 Laker, R.C., Xu, P., Ryall, K.A., Sujkowski, A., Kenwood, B.M., Chain, K.H., Zhang, M., Royal,
980 M.A., Hoehn, K.L., Driscoll, M., Adler, P.N., Wessells, R.J., Saucerman, J.J.,
981 Yan, Z., (2014). A novel mitotimer reporter gene for mitochondrial content, structure, stress, and
982 damage in vivo. J Biol Chem. 2014 Apr 25;289(17):12005-15. DOI: 10.1074/jbc.M113.530527
983
984 Leigh, N.J., Lawton, R.I., Hershberger, P.A., Goniewicz, M.L., (2018). Flavorings significantly
985 affect inhalation toxicity of aerosol generated from electronic nicotine delivery systems (ENDS).
986 Tobacco Control, 25(Suppl 2), ii81, November 2016. DOI:10.1136/tobaccocontrol-2016-053205
987
988 Lin, A.-H., Liu, M., Ko, H., Perng, D., Lee, T., Kou, Y.R., (2018). Menthol cigarette smoke
989 induces more severe lung inflammation than non-menthol cigarette smoke does in mice with
990 subchronic exposure – role of TRPM8. Front Physiol. 2018 Dec 18;9:1817. DOI:
991 10.3389/fphys.2018.01817
992
993 Lisko, J., Stanfill, S., Watson, C., (2014). Analytical methods tobacco products. Anal. Methods
994 6, 4698–4704.
995
996 Liu, Z., Wu, H., Wei, Z., Wang, X., Shen, P., (2016). TRPM8 : a potential target for cancer
997 treatment. J Cancer Res Clin Oncol. 2016 Sep;142(9):1871-81. DOI: 10.1007/s00432-015-
998 2112-1
999
1000 Lloyd, J., O'Malley, P., Miech, R., Bachman, J., Schulenberg, J., (2019). Monitoring the Future
1001 National Survey Results on Drug Use, 1975-2015: Overview, Key Findings on Adolescent Drug
1002 Use. Retrieved from https://eric.ed.gov/?id=ED578539
1003
1004 Miller, E.J., Cohen, A.B., Nagao, S., Griffith, D.E., Maunder, R.J., Martin, T.R., Wiener-Kronish,
1005 J.P., Sticherling, M., Chrisophers, E., Matthay, M.A., (1992). Elevated levels of NAP-
1006 1/Interleukin-8 are present in the airspaces of patients with the adult respiratory distress
1007 syndrome and are associated with increased mortality. Am Rev Respir Dis. 1992
1008 Aug;146(2):427-32. DOI: 10.1164/ajrccm/146.2.427
1009
1010 Muthumalage, T., Prinz, M., Ansah, K.O., Gerloff, J., Sundar, I.K., Rahman, I., (2018).
1011 Inflammatory and oxidative responses induced by exposure to commonly used e-cigarette
1012 flavoring chemicals and flavored e-liquids without nicotine. Front Physiol. 2018 Jan 11;8:1130.
1013 DOI: 10.3389/fphys.2017.01130

Nair, V., Sreevalsan, S., Basha, R., Abdelrahlm, M., Abudayyeh, A., Hoffman, A.R., Safe, S., (2014). Mechanism of metformin-dependent inhibition of mammalian target of rapamycin (mTOR) and Ras activity in pancreatic cancer. J. Biol. Chem. 2014 Oct 3;289(40): 27692–27701. DOI: 10.1074/jbc.M114.592576

National Academies of Sciences, Engineering, and Medicine. 2018. Public Health Consequences of E-Cigarettes. Washington, DC: The National Academies Press. https://doi.org/10.17226/24952.

Nonnemaker, J., Hersey, J., Homsi, G., Busey, A., Allen, J., Vallone, D., (2013). Initiation with menthol cigarettes and youth smoking uptake. Addiction. 2013 Jan;108(1):171-8. DOI: 10.1111/j.1360-0443.2012.04045.x

Omaiye, E.E., Mcwhirter, K.J., Luo, W., Peyton A., Pankow, J.F., Talbot, P. (2019) High concentrations of flavor chemicals are present in electronic cigarette refill fluids. Scientific Reports 9: 2468. https://doi.org/10.1038/s41598-019-39550-2

Omaiye, E.E., Mcwhirter, K.J., Luo, W., Pankow, J.F., Talbot, P., (2018). Toxicity of JUUL fluids and aerosols correlates strongly with nicotine and some flavor chemical concentrations. Chem Res Toxicol. 2019 Jun 17;32(6):1058-1069. DOI: 10.1021/acs.chemrestox.8b00381

Paschke, M., Tkachenko, A., Ackermann, K., Hutzler, C., Henkler, F., Luch, A., (2017). Activation of the cold-receptor TRPM8 by low levels of menthol in tobacco products. Toxicol Lett. 2017 Apr 5;271:50-57. DOI: 10.1016/j.toxlet.2017.02.020

Peace, M.R., Baird, T.R., Smith, N., Wolf, C.E., Poklis, J.L., Poklis, A.J.,(2016) Concentration of Nicotine and Glycols in 27 Electronic Cigarette Formulations. Anal Toxicol. 2016 Jul;40(6):403-7. doi: 10.1093/jat/bkw037.

Peier, A.M., Moqrich, A., Hergarden, A.C., Reeve, A.J., Andersson, D.A., Story, G.M., Earley, T.J., Dragoni, I., Mcintyre, P., Bevan, S., Patapoutian, A., Diego, S., (2002). A TRP channel that senses cold stimuli and menthol. Cell. 2002 Mar 8;108(5):705-15. DOI:10.1016/s0092-8674(02)00652-9

Perkins, N.D., Gilmore, T.D., (2006). Good cop, bad cop: the different faces of NF- KB. Cell Death Differ. 2006 May;13(5):759-72. DOI: 10.1038/sj.cdd.4401838

Poynter, M.E., Irvin, C.G., Janssen-Heininger, Y.M.W., (2002). Rapid activation of nuclear factor- κB in airway epithelium in a murine model of allergic airway inflammation. Am J Pathol. 2002 Apr;160(4):1325-34. DOI: 10.1016/s0002-9440(10)62559-x

Rincon, M., Irvin, C.G., (2012). Role of IL-6 in asthma and other inflammatory pulmonary diseases. Int J Biol Sci. 2012; 8(9): 1281–1290. doi: 10.7150/ijbs.4874

Rizzuto, R., Bernardi, P., Pozzan, T., (2000). Topical review mitochondria as all-round players of the calcium game. J Physiol. 2000 Nov 15;529 Pt 1:37-47. DOI: 10.1111/j.1469-7793.2000.00037.x

Sabnis, A.S., Shadid, M., Yost, G.S., Reilly, C.A., (2008). Human lung epithelial cells express a functional cold-sensing TRPM8 variant. Am J Respir Cell Mol Biol. 2008 Oct;39(4):466-74. DOI: 10.1165/rcmb.2007-0440OC

Saito, Y., Nishio, K., Ogawa, Y., Kimata, J., Kinumi, T., Yoshida, Y., Noguchi, N., Niki, E., (2006). Turning point in apoptosis/necrosis induced by hydrogen peroxide. Free Radic Res. 2006 Jun;40(6):619-30. DOI: 10.1080/10715760600632552

Samanta, K., Douglas, S., Parekh, A.B., (2014). Mitochondrial calcium uniporter MCU supports cytoplasmic Ca2+ oscillations, store-operated Ca2+ entry and Ca2+ -dependent gene expression in response to receptor stimulation. PLoS ONE (Vol. 9, Issue 7) https://doi.org/10.1371/journal.pone.0101188

Scheffler, S., Dieken, H., Krischenowski, O., Aufderheide, M., (2015). Cytotoxic evaluation of e-liquid aerosol using different lung-derived cell models. Int J Environ Res Public Health. 2015 Oct; 12(10): 12466–12474. DOI: 10.3390/ijerph121012466

Stacey, D.W., (2003). Cyclin D1 serves as a cell cycle regulatory switch in actively proliferating cells. Curr Opin Cell Biol. 2003 Apr;15(2):158-63. DOI: 10.1016/s0955-0674(03)00008-5

Symons, M., (1996). Rho family GTPases : the cytoskeleton and beyond. Trends Biochem Sci. 1996 May;21(5):178-81. DOI:https://doi.org/10.1016/S0968-0004(96)10022-0

Takeda, K., Clausen, B.E., Kaisho, T., Tsujimura, T., Terada, N., Forster, I., Akira, S., (1999). Enhanced Th1 activity and development of chronic enterocolitis in mice devoid of Stat3 in macrophages and neutrophils. Immunity. 1999 Jan;10(1):39-49. DOI: 10.1016/s1074-7613(00)80005-9

Teramoto, S., Tomita, T., Matsui, H., Ohga, E., Matsuse, T., Ouchi, Y., (1999). Hydrogen peroxide-induced apoptosis and necrosis in human lung fibroblasts: protective roles of glutathione. Jpn J Pharmacol. 1999 Jan;79(1):33-40. DOI: 10.1254/jjp.79.33

Tierney, P.A., Karpinski, C.D., Brown, J.E., Luo, W., Pankow, J.F., (2016). Flavour chemicals in electronic cigarette fluids. Tob Control. 2016 Apr;25(e1):e10-5. DOI: 10.1136/tobaccocontrol-2014-052175

Tondera, D., Jourdain, A., Karbowski, M., Mattenberger, Y., Cruz, S. Da, Clerc, P., Raschke, I., Merkwirth, C., Ehses, S., Krause, F., Chan, D.C., Alexander, C., Bauer, C., Youle, R., Langer, T., Martinou, J., (2009). SLP-2 is required for stress-induced mitochondrial hyperfusion. EMBO J. 2009 Jun 3;28(11):1589-600. DOI: 10.1038/emboj.2009.89

U.S. Department of Health and Human Services. (2016). E-Cigarette Use Among Youth and Young Adults. A Report of the Surgeon General. Atlanta, GA: U.S. Department of Health and Human Services, Centers for Disease Control and Prevention, National Center for Chronic Disease Prevention and Health Promotion, Office on Smoking and Health, 2016.

Vaart, H.J.D., Murgatroyd, S., Rossiter, H.B., Chen, C., Casaburi, R., Porszasz, J., (2013). Using the power-duration curve to select constant work rates for endurance testing in COPD. American Journal of Respiratory and Critical Care Medicine 2013; 187: A1365

Villanti, A.C., Collins, L.K., Niaura, R.S., Gagosian, S.Y., Abrams, D.B., (2017). Menthol cigarettes and the public health standard: a systematic review. BMC Public Health. 2017 Dec 29;17(1):983. DOI: 10.1186/s12889-017-4987-z

Weng, N.J., Cheung, C., Talbot, P., (2018). Dynamic blebbing: A bottleneck to human embryonic stem cell culture that can be overcome by Laminin-Integrin signaling. Stem Cell Res. 2018 Dec; 33:233-246. DOI: 10.1016/j.scr.2018.10.022

Weng, N.J., Talbot, P., (2017). The P2X7 receptor is an upstream regulator of dynamic blebbing and a pluripotency marker in human embryonic stem cells. Stem Cell Res. 2017 Aug; 23:39-49. DOI: 10.1016/j.scr.2017.06.007

Wieslander, G., Norbäck, D., Lindgren, T., (2001). Experimental exposure to propylene glycol mist in aviation emergency training: acute ocular and respiratory effects. Occup Environ Med. 2001 Oct; 58(10): 649–655. DOI: 10.1136/oem.58.10.649

Willis, D.N., Liu, B., Ha, M.A., Jordt, S., Morris, J.B., (2011). Menthol attenuates respiratory irritation responses to multiple cigarette smoke irritants. FASEB J. 2011 Dec;25(12):4434-44. DOI: 10.1096/fj.11-188383

Wu, H., Goel, V., Haluska, F.G., (2003). PTEN signaling pathways in melanoma. Oncogene. 2003 May 19;22(20):3113-22. DOI: 10.1038/sj.onc.1206451

Xiao, Z., Xue, J., Sowin, T.J., Zhang, H., (2006). Differential roles of checkpoint kinase 1, checkpoint kinase 2, and mitogen-activated protein kinase-activated protein kinase 2 in mediating DNA damage-induced cell cycle arrest: Implications for cancer therapy. Molecular Cancer Therapeutics 5(8):1935-43. DOI: 10.1158/1535-7163.MCT-06-0077.

Yee, N.S., (2015). Roles of TRPM8 ion channels in cancer: proliferation, survival, and invasion. Cancers (Basel). 2015 Oct 23; 7 (4):2134-46. DOI: 10.3390/cancers7040882

Zahedi, A., Phandthong, R., Chaili, A., Remark, G., Talbot, P., (2018). Epithelial-to-mesenchymal transition of A549 lung cancer cells exposed to electronic cigarettes. Lung Cancer. 2018 Aug;122:224-233. DOI: 10.1016/j.lungcan.2018.06.010

Zhang, B., Shan, H., Li, D., Li, Z., Zhu, K., (2012). Different methods of detaching adherent cells significantly affect the detection of TRAIL receptors. Tumori 98, 800–803. DOI: 10.1700/1217.13506

Zhao, W., Xu, H., (2016). High expression of TRPM8 predicts poor prognosis in patients with osteosarcoma. Oncol Lett. 2016 Aug;12(2):1373-1379. DOI: 10.3892/ol.2016.4764

Zhao, Y., Du, L., Du, G., (2018). Menthol. natural small molecule drugs from plants [981-10-8021-6; 981-10-8022-4] pg:289 -294

Figures

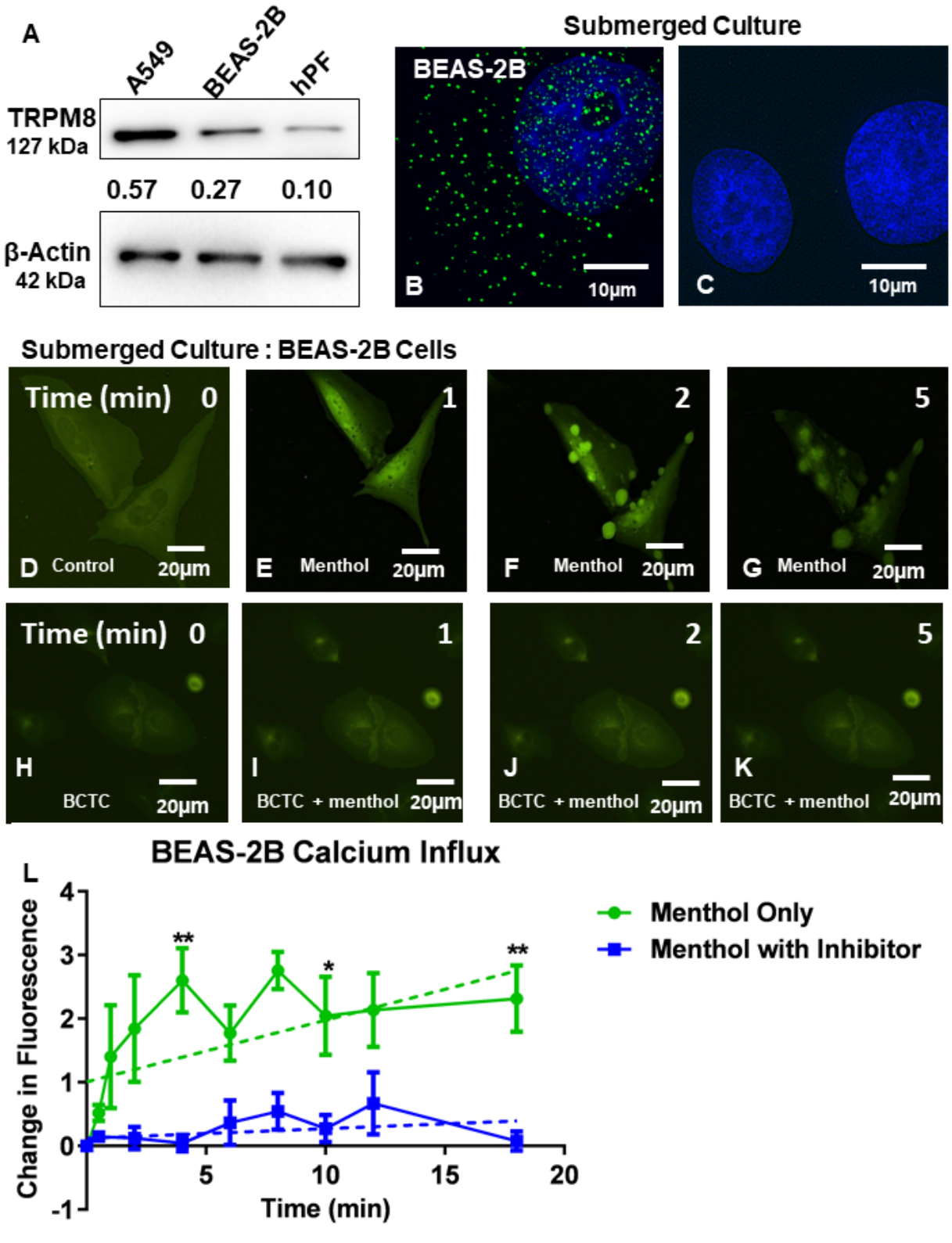
A
A549
BEAS-2B
hPF
TRPM8
127 kDa
0.57
0.27
0.10
β-Actin
42 kDa
Submerged Culture
BEAS-2B
B
10μm
C
10μm
Submerged Culture : BEAS-2B Cells
Time (min) 0
D Control 20μm
1
E Menthol 20μm
2
F Menthol 20μm
5
G Menthol 20μm
Time (min) 0
H BCTC 20μm
1
I BCTC + menthol 20μm
2
J BCTC + menthol 20μm
5
K BCTC + menthol 20μm
L
BEAS-2B Calcium Influx
Change in Fluorescence
Time (min)
Menthol Only
Menthol with Inhibitor
**
*
**

Figure 1. Menthol Induces Calcium Influx via the TRPM8 Receptor in Submerged Cultures of BEAS-2B Cells

(A) TRPM8 western blot of A549 cells, BEAS-2B cells, and hPFs with β-actin as the loading control. (N=1)

(B-C) Immunocytochemical staining of BEAS-2B cells with a human TRPM8 antibody (B), and negative control treated with secondary antibody alone (C). The nuclei were counterstained using DAPI. This experiment was performed three times.

(D-K) Time-lapse micrographs of BEAS-2B cells transfected with the GCaMP5 plasmid and treated with 0.2 mg/mL (1.3 mM) of pure menthol (D-G) and TRPM8 inhibitor (BCTC) (H) plus menthol (I-K). This experiment was performed three times.

(L) Graph showing changes in fluorescence intensity in menthol-treated cells with and without the TRPM8 inhibitor. A two-way ANOVA was performed by comparing change in green fluorescence versus time, and significant changes in green fluorescence are indicated by ** and * for $p < 0.01$ and $p < 0.05$, respectively. Each point is the mean of three independent experiments ± the SEM.

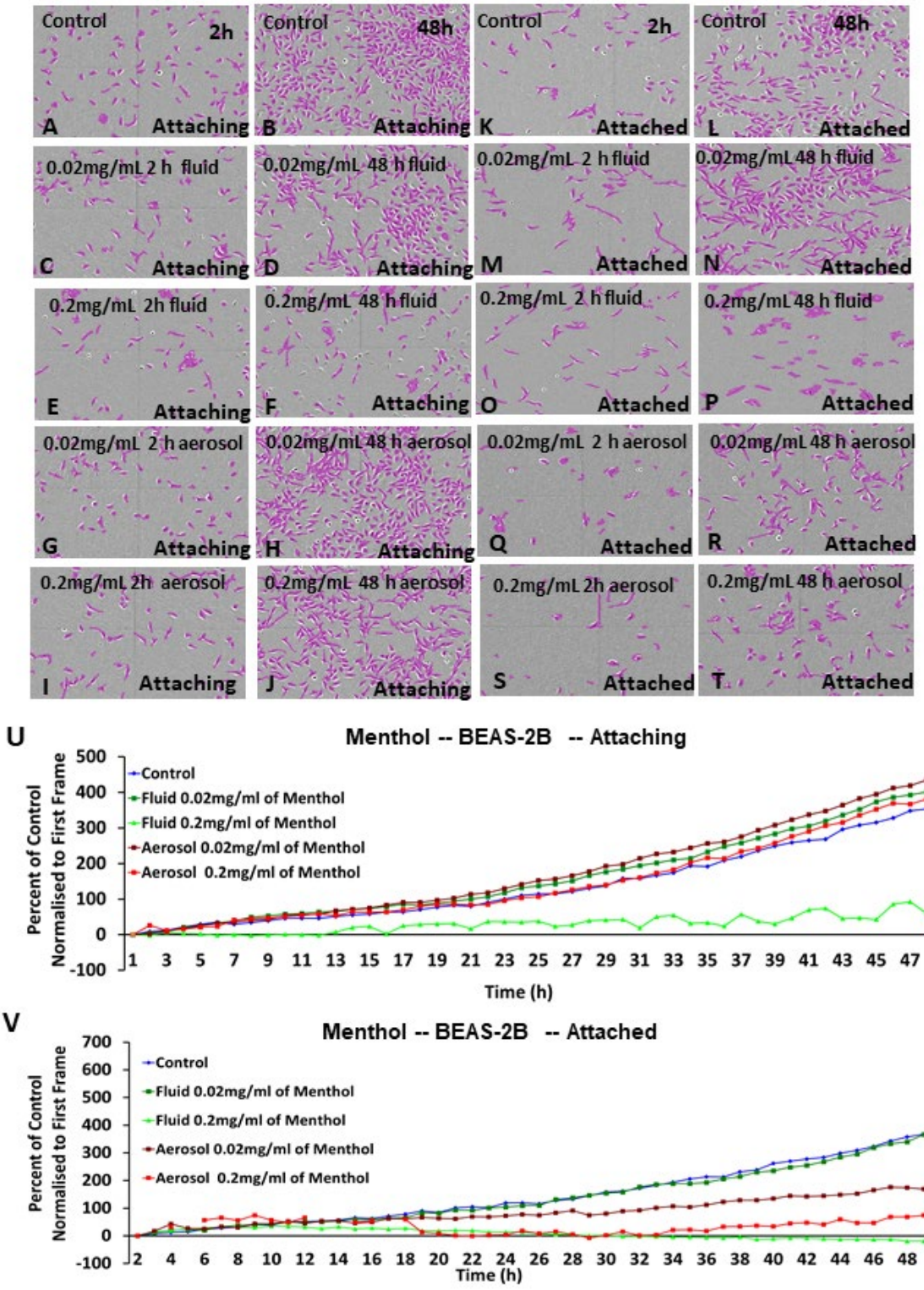

Figure 2. Effect of Menthol Fluids and Aerosol Fluids on Proliferation of BEAS-2B Cells in Submerged Culture.

(A-T) Micrographs of BEAS-2B cells treated with menthol fluid (0.02 mg/mL or 0.2 mg/mL) and menthol aerosol fluid (0.02 mg/mL and 0.2 mg/mL) during plating (A-J attaching) and 24 h after plating (K-T attached). Cells were imaged live in a Nikon BioStation CT, and time-lapse images were captured every 2 h for 48 h. Cells have been segmented with CL-Quant software and colorized to show their boundaries clearly.

(U and V) Graphs showing confluency of treated cells normalized to untreated controls versus time in control and treatment groups. Data are plotted as means of 2 experiments.

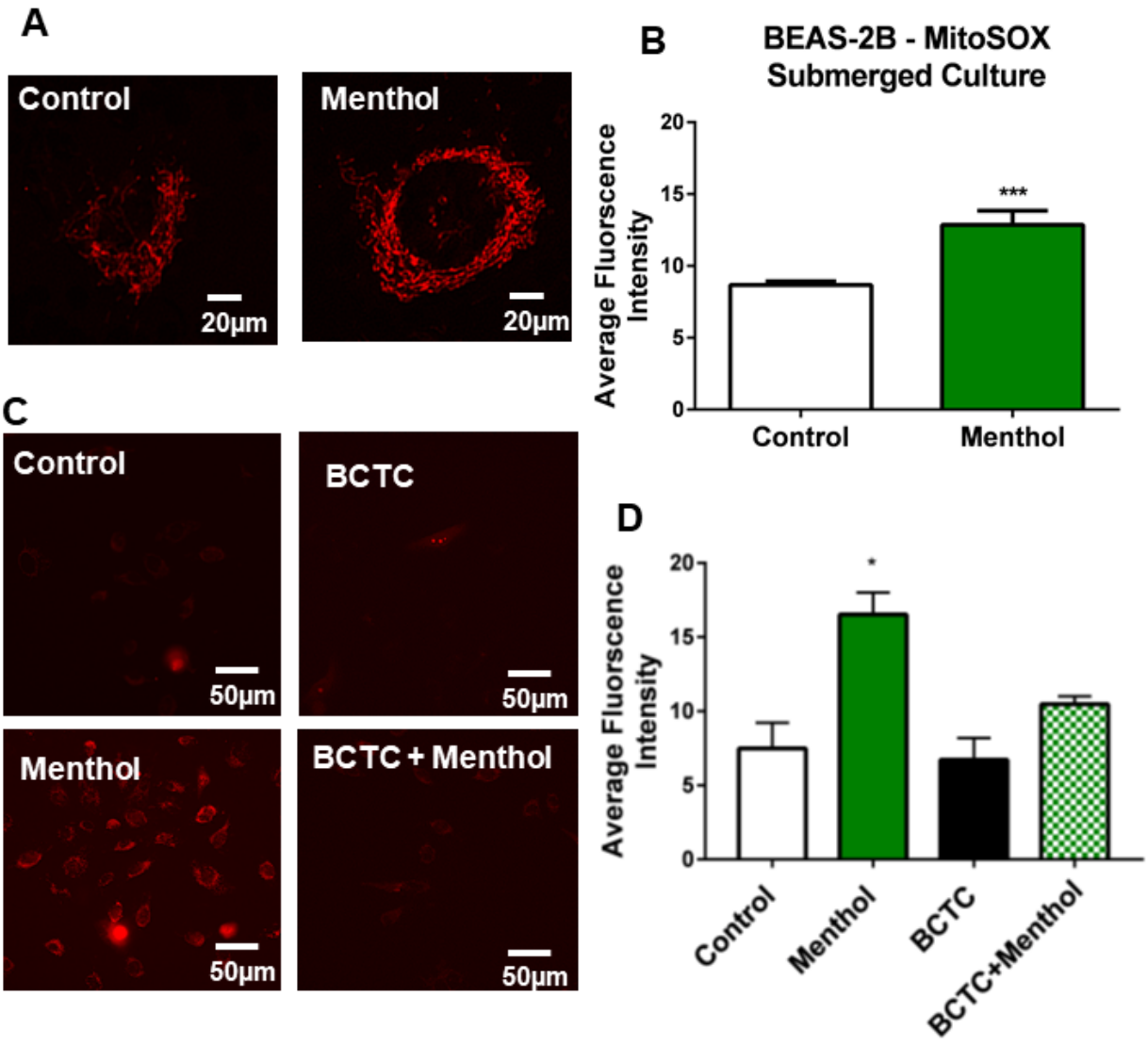

1188

1189 **Figure 3. Mitochondrial ROS Generation in Menthol-treated BEAS-2B Cells in Submerged**

1190 **Culture.**

(A) Micrographs of BEAS-2B cells labeled with MitoSOX-Red after no treatment (control) or treatment with 0.2 mg/mL menthol.

(B) Graph showing average fluorescence intensity per cell in control and menthol-treated cells. A two tailed t-test was used to compare fluorescent intensity. In B, each bar is the mean of three independent experiments ± the SEM. Duplicate wells were averaged in each experiment. *** = $p<0.0001$

(C and D) Effects of menthol on BEAS-2B cells after blocking the TRPM8 receptor with BCTC. Cells were labeled with MitoSOX-Red after menthol treatment (4 h) with and without TRPM8 inhibitor (BCTC). Statistical significance was determined using a one-way ANOVA and significant changes were isolated using Dunnett's posthoc test in which each group was compared to the untreated control. In D, each bar is the mean of three independent experiments ± the SEM. Duplicate wells were averaged in each experiment. * = $p < 0.05$; *** = $p<0.0001$.

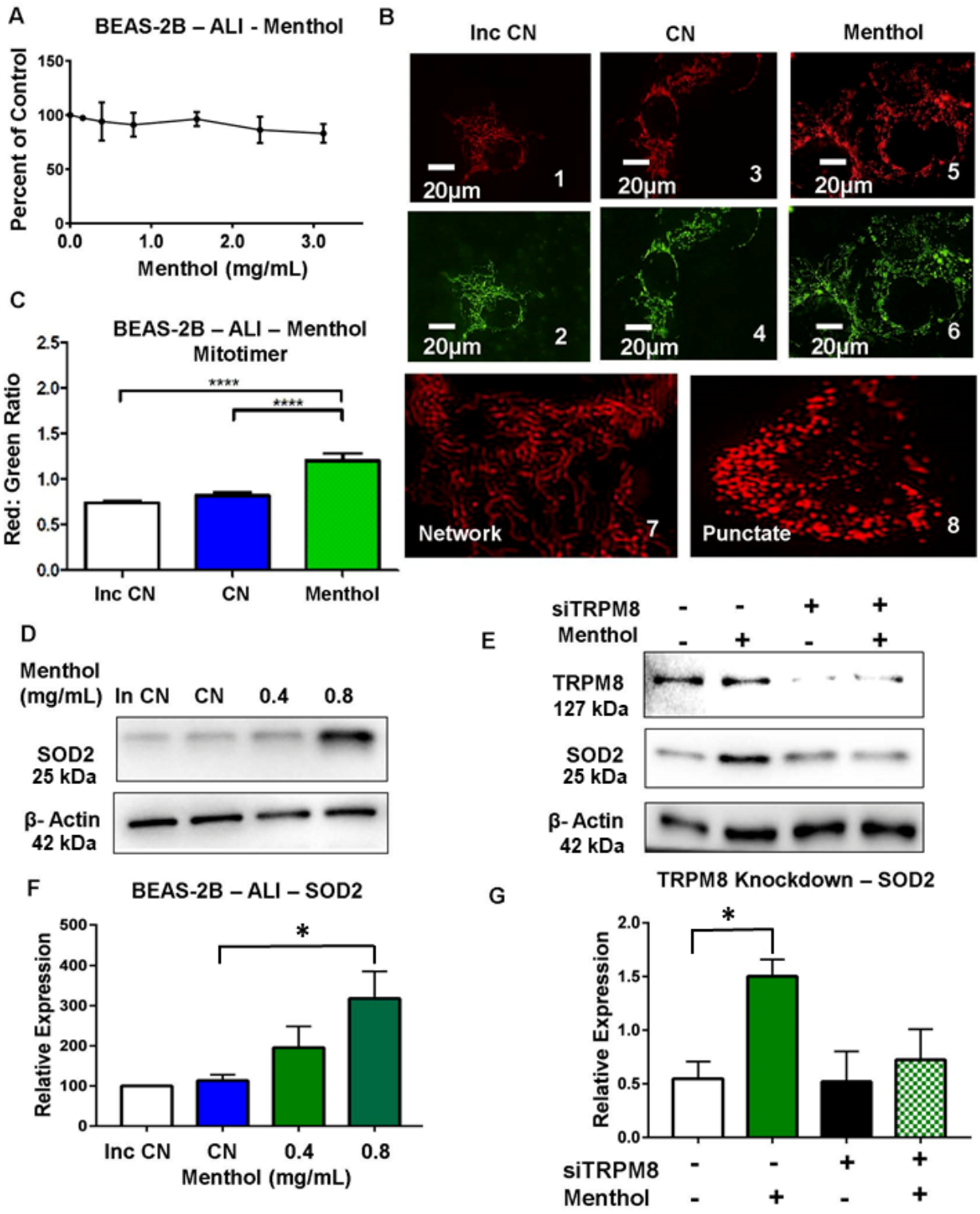

1205

1206 **Figure 4. Menthol Exposure at the ALI in a Cloud Chamber Induced an Oxidative Stress**

1207 **Response and Elevation of an Antioxidant Enzyme.**

(A) MTT dose-response curve showing absorbance (percent of control) plotted as a function of different concentrations (0.15 – 3.125 mg/mL) of menthol aerosol in ALI exposure. Monolayers of BEAS-2B cells were used in all experiments. Each bar is the mean of three independent experiments ± the SEM. Duplicate wells were averaged in each experiment.

(B) Fluorescent micrographs of BEAS-2B cells transfected with MitoTimer plasmid. (1, 2) are micrographs of the incubator control, (3, 4) are control aerosol exposure and (5, 6) are menthol aerosol exposure. (7, 8) are magnified images showing networked and punctate mitochondria before and after menthol treatment.

(C) The red/green ratio of the MitoTimer expressing cells is plotted for each group. Each bar is the mean of three independent experiments ± the SEM. Duplicate wells were averaged in each experiment. A one-way ANOVA was used to compare means. **** = $p < 0.00001$

(D) Expression of SOD2 in BEAS-2B cells exposed to menthol aerosol (0.4 mg/mL and 0.8 mg/mL). β-actin was used as the loading control. Inc CN is the incubator control, and CN is the control exposed to 1% DMSO.

(E) BEAS-2B cells were treated with siRNA against TRPM8 and exposed to menthol aerosol. Whole cell lysates were then analyzed by western blot for expression of SOD2. β-actin was used as the loading control

(F and G) Relative expression of SOD2 in western blots D and E, respectively. Bars in F and G are means of three independent experiments and error bars represent the SEM. Duplicate wells were averaged in each experiment. A one-way ANOVA with Dunnett's posthoc test was used to compare means in the knockdown experiment. * = $p < 0.05$, ** = $p<0.01$. In F, only the 0.8 mg/ml of menthol significantly increased expression of

SOD2. In G, only the menthol treated group was significantly higher than the untreated control.

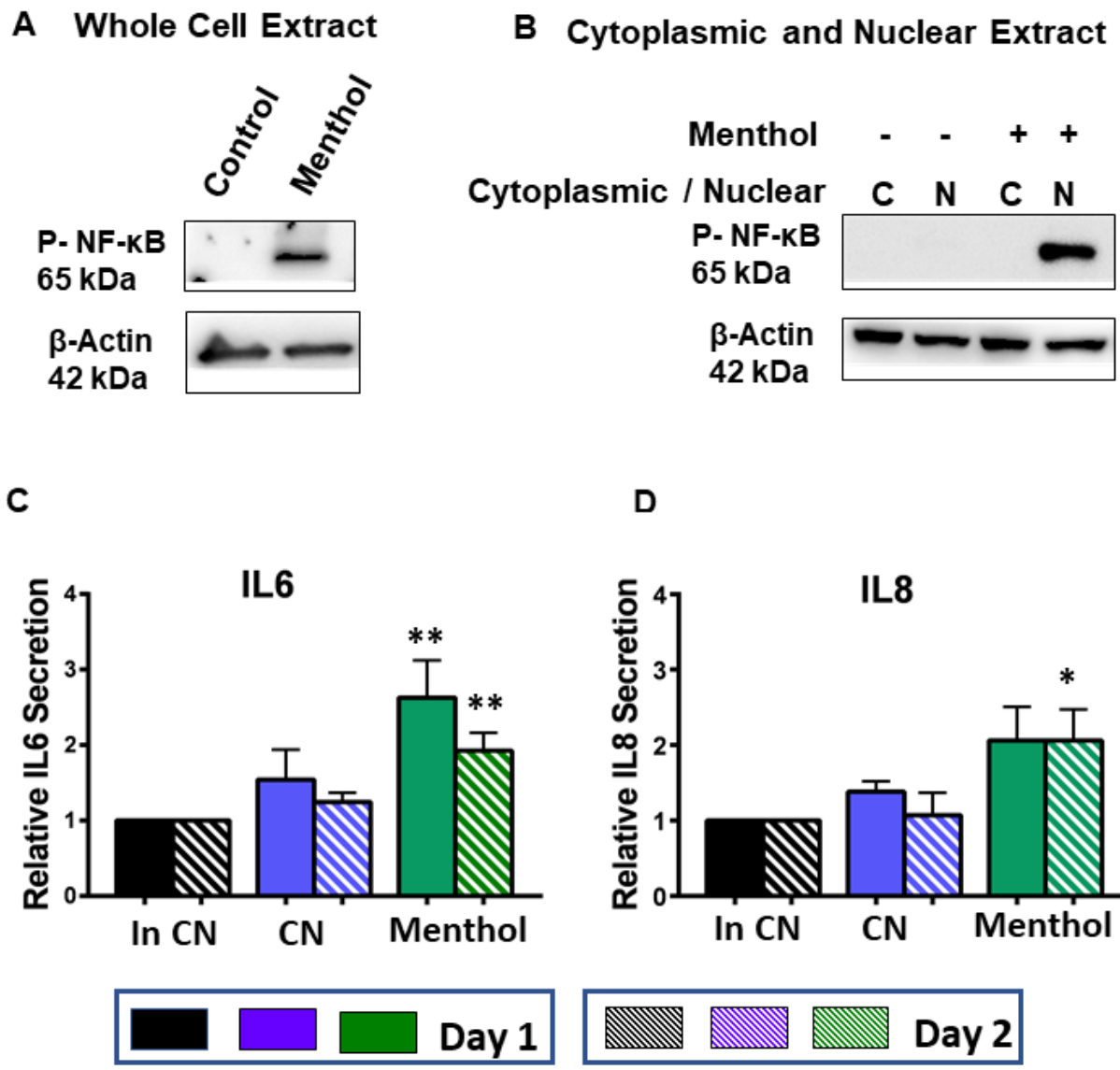
A Whole Cell Extract
Control
Menthol
P- NF-κB
65 kDa
β-Actin
42 kDa
B Cytoplasmic and Nuclear Extract
Menthol - - + +
Cytoplasmic / Nuclear C N C N
P- NF-κB
65 kDa
β-Actin
42 kDa
C
IL6
Relative IL6 Secretion
0
1
2
3
4
**
**
In CN
CN
Menthol
Day 1
D
IL8
Relative IL8 Secretion
0
1
2
3
4
*
In CN
CN
Menthol
Day 2

Figure 5. ALI Exposure to Menthol Aerosol in the Cloud Chamber Stimulated Activation of NF-kB and Increased Secretion of Immunomodulatory Cytokines in BEAS-2B cells.

(A and B) Western blot showing expression of phospho-NF-kB in whole cell extract (A) and in nuclear and cytoplasmic extracts (B) of BEAS-2B cells exposed to menthol aerosol (0.8 mg/mL) in a cloud chamber. β-actin was used as the loading control.

(C and D) IL-6 levels (Day1 and Day2) and IL-8 (Day1 and Day2) levels in the culture medium, measured by ELISA. Following menthol exposure in the ALI chamber, medium was collected after 24 h (Day 1), replaced with fresh medium, and collected again 24 h later (Day 2). Bars in C and D are the means ± SEM of three independent experiments. Duplicate wells were averaged in each experiment. Statistical significance was determined using one-way ANOVA with Dunnett's posthoc test. * = $p < 0.05$; ** = $p < 0.01$.

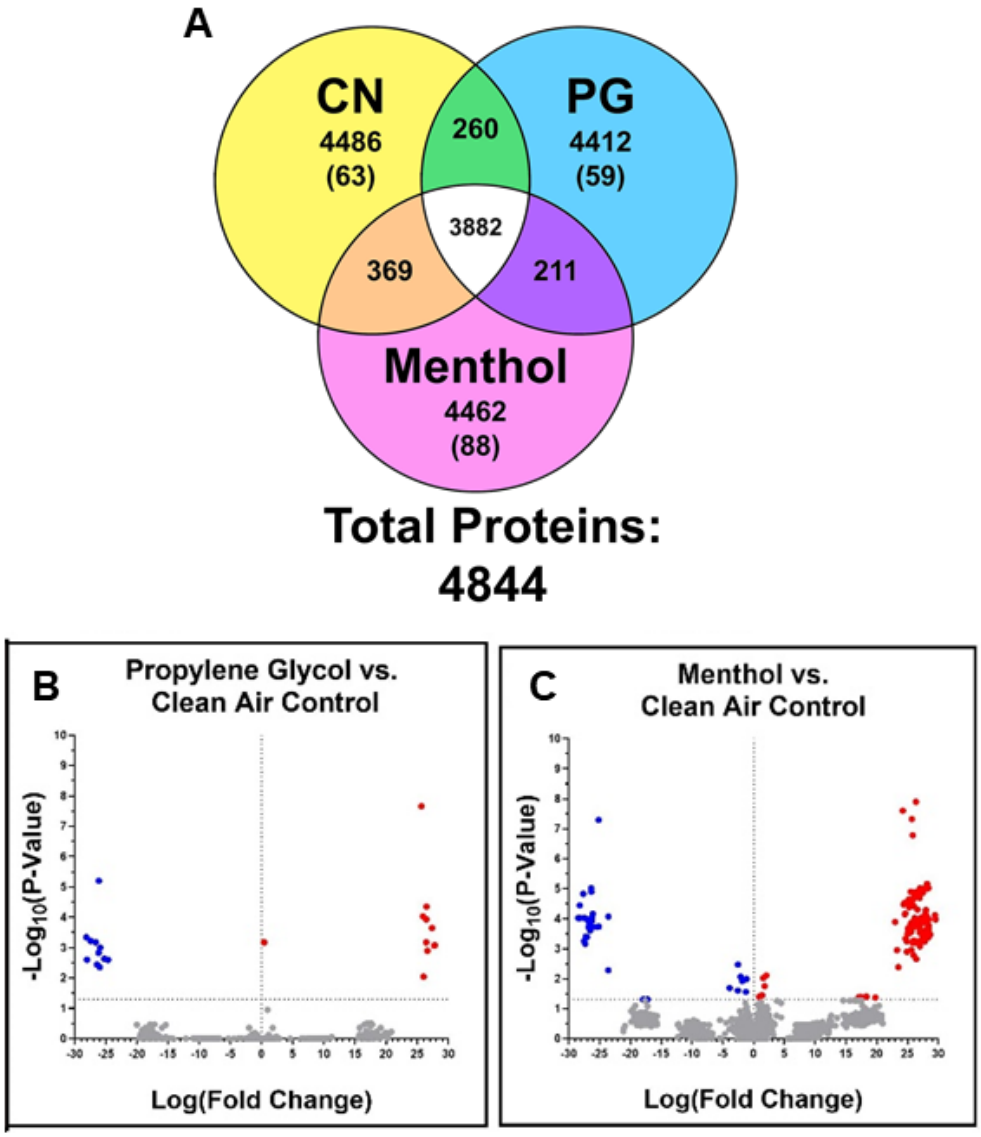

Figure 6. Identification of Proteins Affected by ALI Exposure of EpiAirway Tissue to Menthol or PG Aerosol in the Cultex System.

(A) Venn diagram of overlapping proteins identified in each treatment group. Values above the parentheses indicate all proteins detected after treatment, while values in parentheses are proteins unique to the CN, PG, and menthol groups.

(B) Volcano plot showing proteins significantly changed in the PG group relative to the clean air controls.

(C) Volcano plot showing proteins significantly changed in the menthol group relative to the clean air controls.

In B and C, horizontal dashed lines indicate $p < 0.05$. Blue and red dots show down and up regulated proteins, respectively.

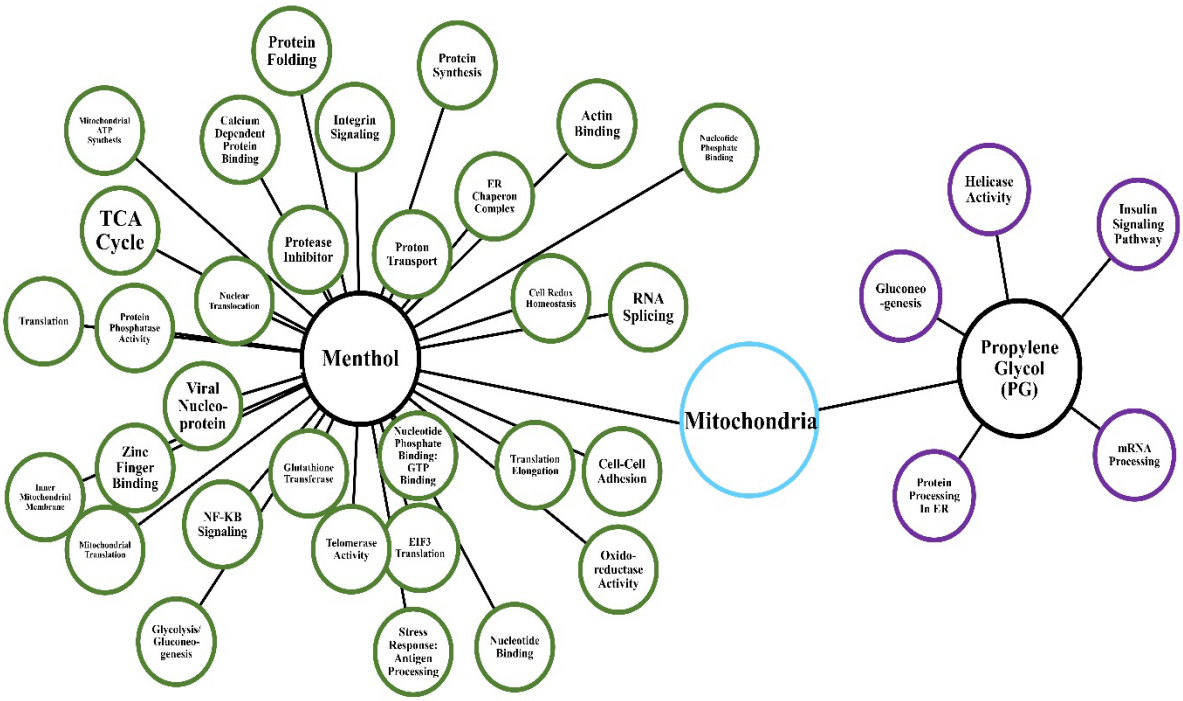

Figure 7. DAVID Derived Interactome of Enrichment Clusters in EpiAirway Tissues Exposed to Menthol or PG at the ALI in the Cultex System

Interaction diagram of proteomics data analyzed with DAVID annotation clustering (p-value <0.05). Only significant proteins with adjusted p-value <0.05 after statistically isolating the effect of PG vehicle were considered for menthol. All proteins significant relative to the Clean Air control (CA) were considered for PG vehicle control.

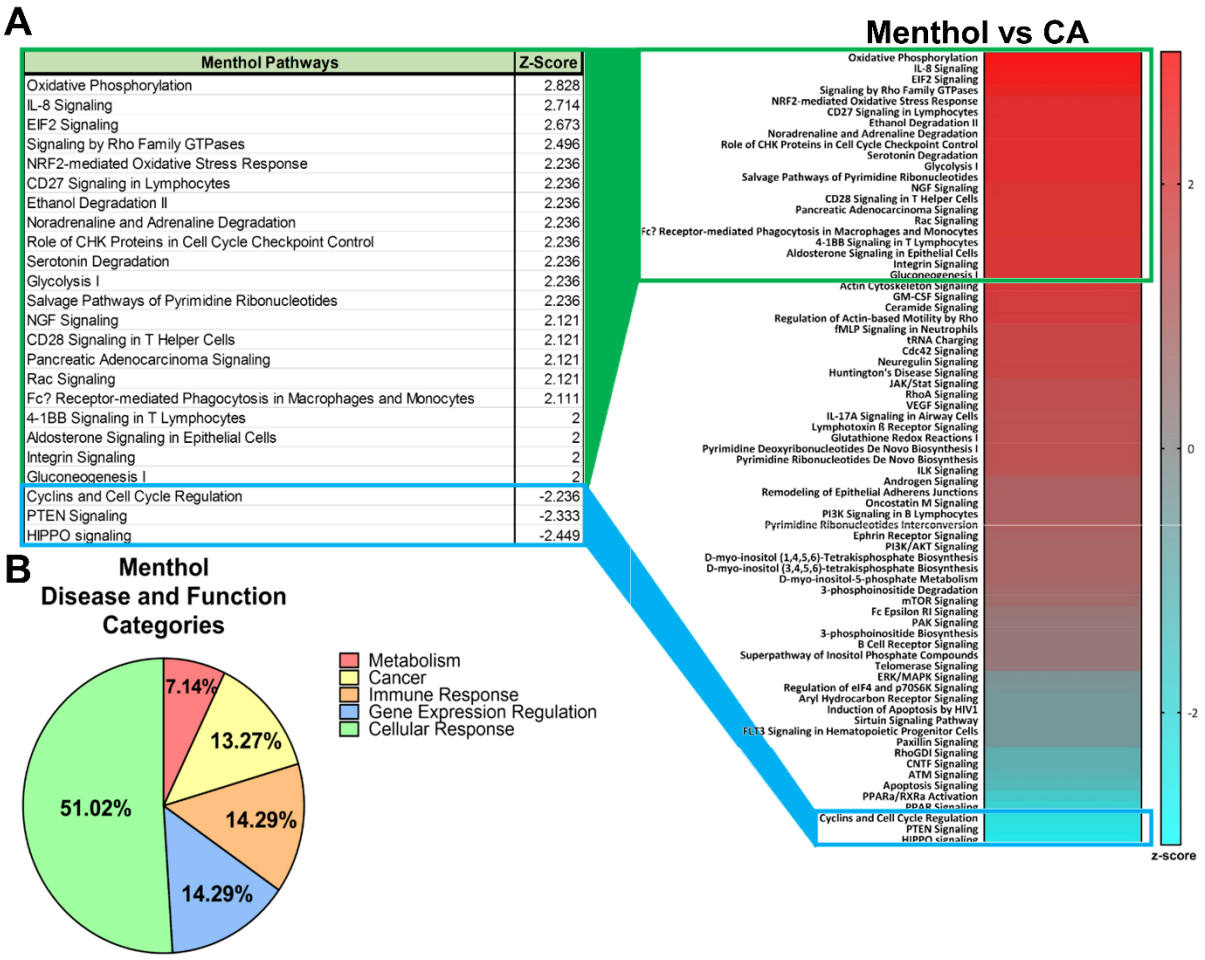

Figure 8. IPA Pathway Analysis and Protein Association Annotations Following 3D Cultex Exposure of EpiAirway at the ALI

(A) Heat map of canonical pathways identified with IPA with table of significantly affected pathways (Z-Score>=2; Z-Score<=-2) after Cultex exposure to aerosol from a menthol EC normalized to the Clean Air control (CA).

(B) Frequency of proteins associated with disease or function identified by IPA in the menthol-treated group. Only proteins with adjusted p-values <0.05 after statistical modeling to isolate the effect of PG vehicle were considered.

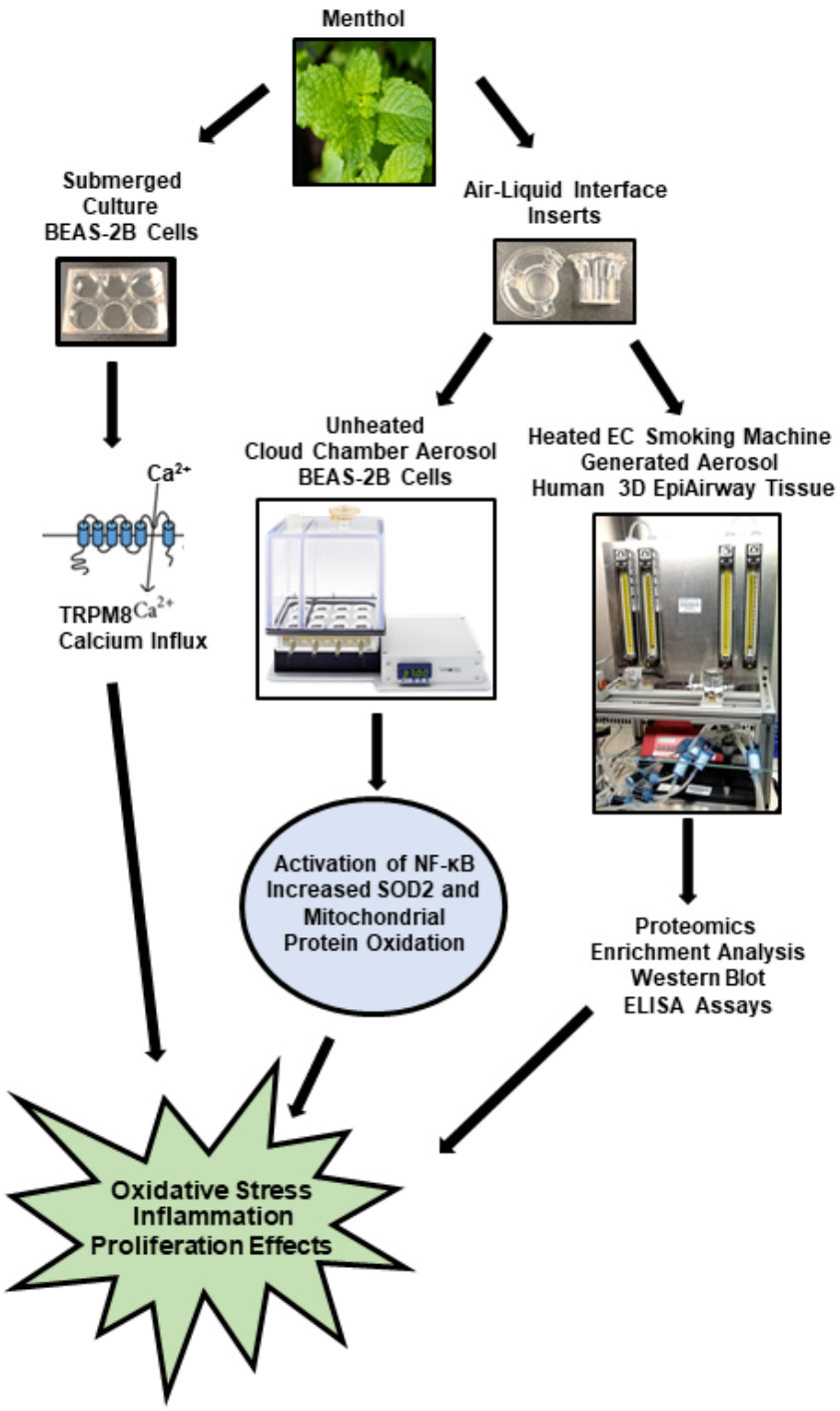

1282

1283 **Graphical Abstract. Mechanism of action of menthol on human bronchial epithelium.**

1284 Three *in vitro* platforms were used to study the effect of menthol on bronchial epithelium. In

1285 submerged culture (using BEAS-2B cells), menthol produced rapid calcium influx followed by an

increase in oxidative stress and inflammatory cytokines. ALI exposure of BEAS-2B cells to unheated menthol in a cloud chamber caused activation of an inflammatory transcription factor (NF-κB) and oxidative stress. Proteomics analysis of human EpiAirway tissues exposed at the ALI to heated menthol EC aerosols identified changes in the expression of proteins involved in oxidative stress and in an inflammatory response.

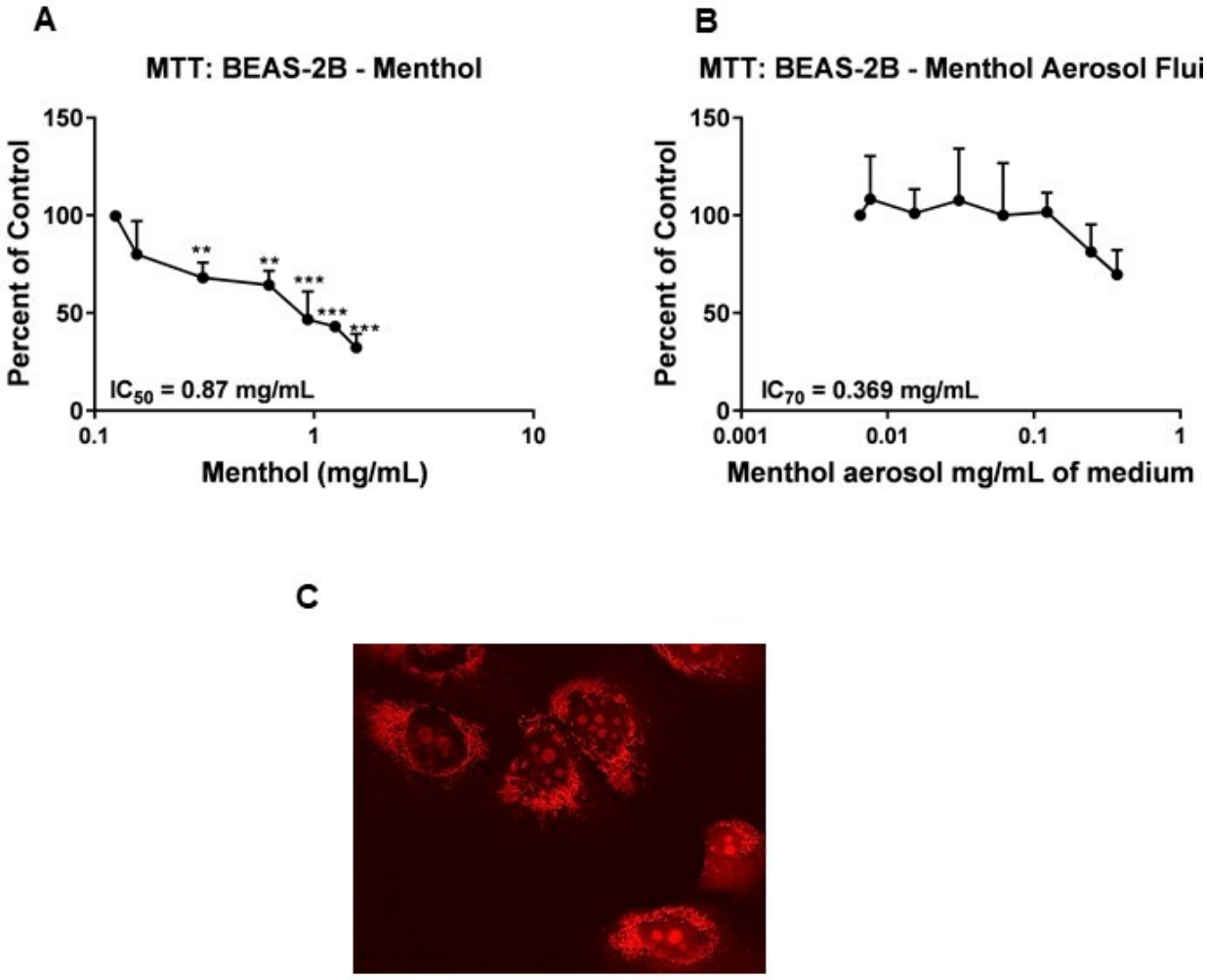

Supplementary Figure 1. MTT assay of submerged BEAS-2B cells after exposure to menthol and positive control for the MitoSOX assay

(A and B) Analysis of cell metabolism during submerged exposure of BEAS-2B cells using menthol fluid (A) and menthol aerosol fluid (B). Cell metabolism is expressed relative to the control. Data are plotted as means of three independent experiments ± SEM. Statistical significance was determined with GraphPad Prism using a one-way ANOVA. When significance was found, treated groups were compared with the lowest concentration using Dunnett's post hoc test. A two-tailed t-test was used to analyze the migration efficiency in the transwell assay. * = $p < 0.05$; ** = $p < 0.01$; *** = $p<0.001$.

(C) Positive control for MitoSOX assay. Micrographs of BEAS-2B cells labeled with MitoSOX-Red after treatment with 500 nM of rotenone.

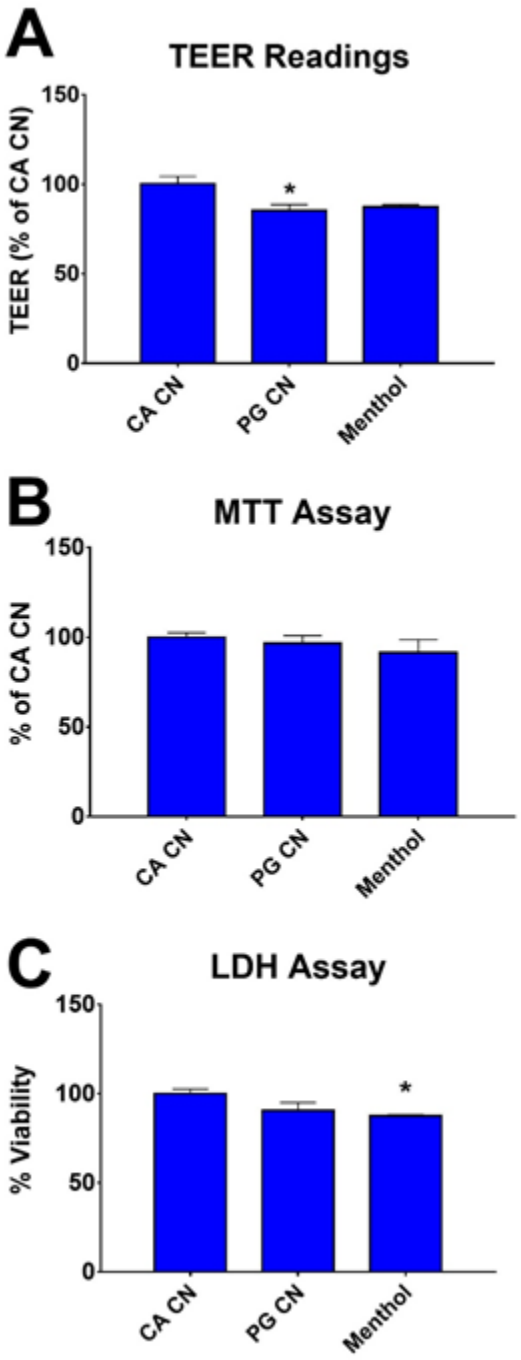

Supplementary Figure 2. Cytotoxicity Assays on 3D EpiAirway Tissues after exposure to Menthol Aerosols

(A) TEER Assay as percent of Clean Air Control.

(B) MTT Assay as percent of Clean Air Control

(C) LDH Assay as percent of Clean Air Control. Statistical significance was determined with GraphPad Prism using a one-way ANOVA for all assays. When significance was found, treated groups were compared with the Clean Air Control using Dunnett's post hoc test. * = $p < 0.05$

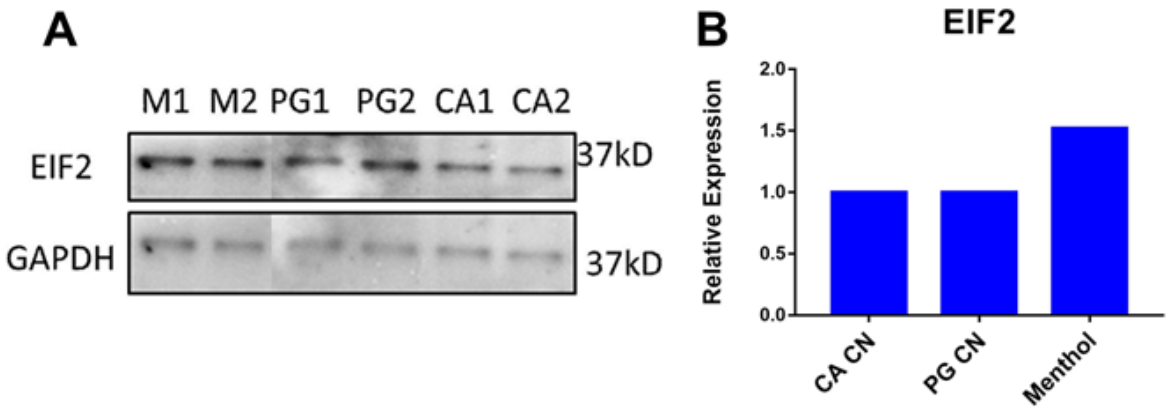

Supplementary Figure 3. Validation of Proteomic Results on 3D EpiAirway Tissue lysates after exposure in Smoking Machine

(A) Western Blot of eIF2 in duplicate after exposure to menthol (M1 and M2), propylene glycol (PG1 and PG 2), or Clean Air (CA1 and CA1) in smoking machine.

(B) Intensity of western blots quantified with ImageJ and plotted with relative expression to Clean Air control.

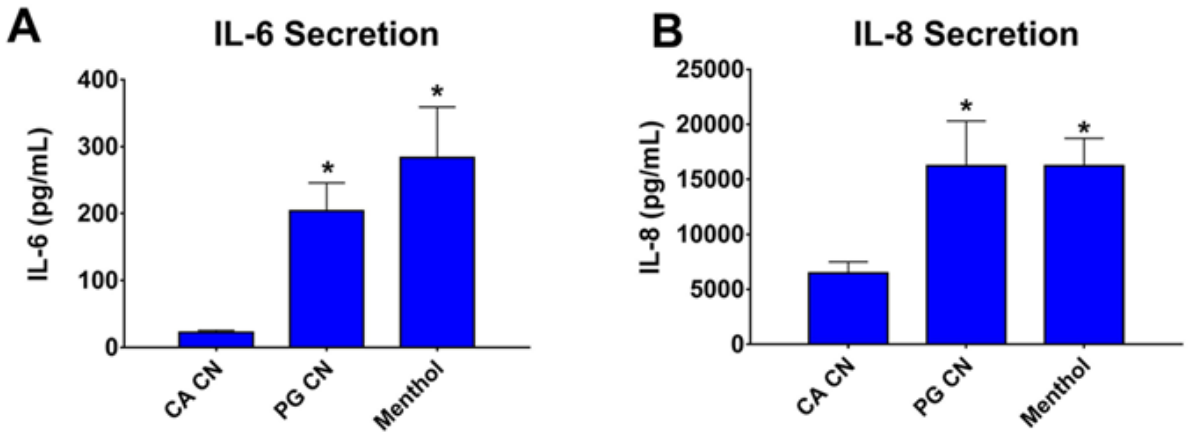

Supplementary Figure 4. Secretion of cytokines by 3D EpiAirway Tissue into cell media after a 24hr recovery period

(A) IL-6 secretion in pg/mL.

(B) IL-8 Secretion in pg/mL. Statistical significance was determined with GraphPad Prism using a one-way ANOVA for all assays. When significance was found, treated groups were compared with the Clean Air Control using Dunnett's post hoc test. * = $p < 0.05$

Supplementary Video 1. Menthol induced calcium flux: Time-lapse video of BEAS-2B cells transfected with GCaMP5 showing calcium in control and menthol-treated cells.

(A) 5-minute time course of transfected BEAS-2B cells treated with cell media

(B) 5-minute time course of transfected BEAS-2B cells treated with menthol